Tetrameric UvrD helicase is located at the *E. coli* replisome due to frequent replication blocks

Adam J. M Wollman[1,2,3,], Aisha H. Syeda[1,2], Jamieson A. L. Howard[1,2], Alex Payne-Dwyer[1,2], Andrew Leech[4] , Colin Guy[5, 6], Peter McGlynn[2,6], Michelle Hawkins[2] and Mark C. Leake[1,2]

The authors wish it to be known that, in their opinion, the first two authors should be regarded as joint First Authors

[1] School of Physics, Engineering and Technology, University of York, York YO10 5DD, United Kingdom.

[2] Department of Biology, University of York, York YO10 5DD, United Kingdom.

[3] Current address: Biosciences Institute, Newcastle University, NE1 7RU, United Kingdom.

[4] Bioscience Technology Facility, Department of Biology, University of York, York YO10 5DD, United Kingdom

[5] Current address: Covance Laboratories Ltd., Otley Road, Harrogate, HG3 1PY, United Kingdom

[6] Previous address: School of Medical Sciences, Institute of Medical Sciences, University of Aberdeen, Foresterhill, Aberdeen AB25 2ZD, United Kingdom

* To whom correspondence should be addressed. To whom correspondence should be addressed. Tel: +44 (0)1904322697. Email: mark.leake@york.ac.uk

Present Address: School of Physics, Engineering and Technology, and Department of Biology, University of York, York YO10 5DD, United Kingdom

SUMMARY

DNA replication in all organisms must overcome nucleoprotein blocks to complete genome duplication. Accessory replicative helicases in *Escherichia coli*, Rep and UvrD, help replication machinery overcome blocks by removing incoming nucleoprotein complexes or aiding the re-initiation of replication. Mechanistic details of Rep function have emerged from recent live cell studies; however, the division of UvrD between its multiple activities in DNA repair and its role as an accessory helicase remains unclear in live cells. Here, by integrating super-resolved single-molecule fluorescence microscopy with biochemical analysis, we find that UvrD self-associates into tetrameric assemblies and, unlike Rep, is not recruited to a specific replisome protein despite being found at approximately 80% of replication forks. Instead, its recruitment to forks is likely mediated by the very high frequency of replication blocks due to DNA bound proteins, including RNA polymerase and DNA damage. Deleting *rep* and DNA repair factor genes *mutS* and *uvrA*, and inhibiting transcription through

RNA polymerase mutation and antibiotic inhibition, indicates that the level of UvrD at the fork is dependent on its function. Our findings show that UvrD is recruited to sites of nucleoprotein blocks via different mechanisms to Rep and plays a multi-faceted role in ensuring successful DNA replication.

INTRODUCTION

Replication and transcription of DNA occur simultaneously in *Escherichia coli,* making conflicts between the bacterial replisome, the molecular replication machine comprising in excess of 10 different proteins, and RNA polymerase (RNAP) inevitable (1–4). Collisions between the replication and transcription machineries hinder replication fork progression and cause genome instability (5–14). RNAP can pause, stall and backtrack while actively transcribing, and any immobile RNAP molecules present long-lived barriers to replisomes (15, 16). These factors make RNAP the most common nucleoprotein obstacle for translocating replisomes. DNA is also frequently damaged in normal growth conditions due to exposure to endogenous and exogenous DNA damaging agents. The resulting DNA damage also presents significant obstacles for normal replication (17–19).

Several mechanisms exist to reduce conflict between the replisome and obstacles such as transcribing RNAPs. For example, transcription elongation and termination factors reduce the number of immobile RNA polymerases on DNA (1, 18, 20–24). Head-on collisions were originally thought to be more harmful (25–27) and therefore more important to resolve; a view supported by the occurrence of highly transcribed genes encoded on the leading strand, presumably to ensure co-directional transcription and replication (26, 28, 29). However, co-directional collisions of the replisome and transcription machinery also impact replication fork progression (3, 18, 30).

Accessory replicative helicases promote fork movement through nucleoprotein barriers and have been identified in prokaryotes and eukaryotes (1, 12, 13, 31, 32). The Rep and UvrD accessory helicases in *E. coli*, as well as the Pif1 helicase in *Saccharomyces cerevisiae*, perform important roles in helping to clear nucleoprotein complexes (33). More recently, Pif1 has been proposed to be a general displacement helicase for replication bypass of protein blocks, a function similar to the Rep and UvrD helicases (34). These helicases can reduce replisome pausing at several types of

native transcription complexes observed in living cells (13, 22, 35), and several types of engineered nucleoprotein blocks in biochemical experiments *in vitro* (1, 31).

Rep is the primary accessory helicase in *E. coli*, however, UvrD can partially compensate for the absence of Rep *in vivo* and has been shown to promote replication through stalled transcription elongation complexes (1, 12, 13, 36, 37). UvrD is a superfamily 1 helicase that translocates 3'-5' along ssDNA. The ability of UvrD to compensate partially for the absence of Rep has been attributed to the high degree of homology between these two helicases and the abundance of UvrD inside cells (12, 21, 38–40). The role of UvrD in nucleotide excision repair along with UvrABC proteins as well as in methyl-directed mismatch repair along with the MutHLS proteins is well characterised (41–46). UvrD interacts directly with RNAP but the functional importance of this interaction has been unclear until recently (47–50). UvrD has been suggested to promote backtracking of stalled RNAP as a first step in transcription-coupled repair (50, 51); however, other studies argue against UvrD playing any role in coupling nucleotide excision repair to stalled transcription complexes (48, 49, 52–56).

Here, we combined state-of-the-art *in vivo* imaging using single-molecule microscopy with advanced biochemical activity and imaging experiments *in vitro* to elucidate how UvrD resolves replicative blocks. We used super-resolved high-speed single-molecule fluorescence microscopy of mGFP-UvrD in live cells co-expressing a fork marker, DnaQ-mCherry, to reveal that 80% of DnaQ foci colocalise with UvrD. Stepwise photobleaching intensity analysis revealed tetrameric UvrD foci *in vivo*, to be compared with earlier observations performed *in vitro* using analytical ultracentrifugation that found a mixture of UvrD dimers and tetramers (57). Surface plasmon resonance (SPR) measurements of UvrD in combination with each replisome component identified no specific replisome protein interaction partner that would explain replisome-UvrD colocalisation. Deletion of Rep, mismatch repair protein MutS and nucleotide excision repair protein UvrA, and disruption of transcription using either mutation of RNAP or antibiotic inhibition, significantly reduces the number of UvrD or level of observed colocalisation of UvrD with the fork. Coupled with *in vitro* block-dependent differences in UvrD replication promotion efficiency, we conclude that UvrD is most likely located at the *E. coli* replisome due to its role in resolving frequent blocks to replication.

RESULTS

UvrD is present at the majority of replication forks

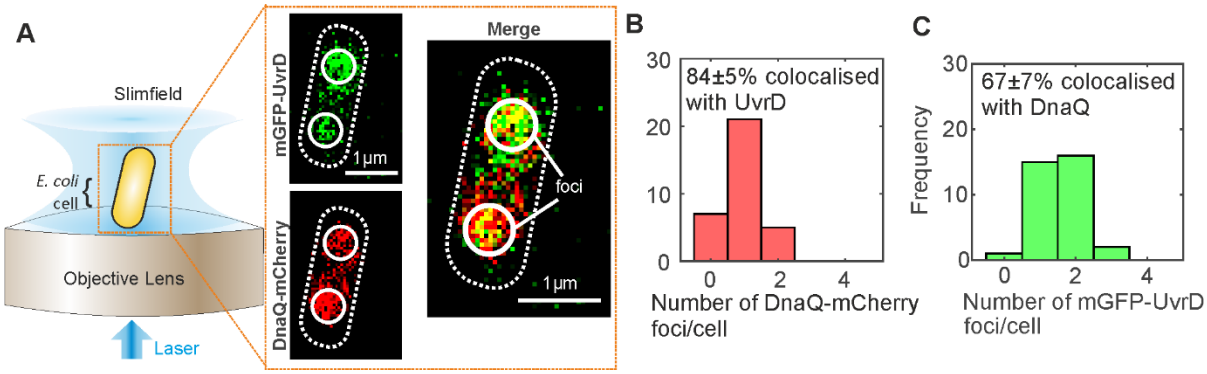

Figure 1: Super-resolved single-molecule light microscopy. (A). Slimfield microscope schematic and Slimfield micrographs of mGFP-UvrD, DnaQ-mCherry. Cell membrane and DnaQ/UvrD foci indicated as white dashed and non-dashed lines respectively. (B) and (C) Histogram showing the number of DnaQ and UvrD foci detected per cell respectively, SD errors. N=45 cells.

We investigated the role of UvrD in DNA replication using super-resolved single-molecule fluorescence microscopy to track dynamic patterns of fluorescently labelled UvrD localization relative to the replication fork in live cells (Figure 1A). We performed dual-colour Slimfield (58, 59) to assess the degree of colocalisation between UvrD and the replisome, using the same imaging protocol we used previously to confirm Rep colocalisation with the replisome (13). We employed DnaQ-mCherry as a fork marker (13) along with a genomically integrated mGFP-UvrD fluorescent protein fusion construct to report on the localization of UvrD. DnaQ encodes the epsilon subunit, a core component of the DNA polymerase and is well established as a marker for the replication fork (13, 60–63). These strains phenocopied the wild type strain for growth and in plasmid loss assays testing for mGFP-UvrD function retention (Supplementary Figures S1, S2, Tables S1-4). The helicase activity of mGFP-UvrD was comparable to the wild type enzyme in an *in vitro* unwinding assay (Supplementary Figure S3). Under Slimfield, we observed 1-2 DnaQ foci as in the previous study for Rep, corresponding to the two moving replication forks which appear as single foci near the start of replication when they are separated by less than the 200-300 nm diffraction limit of our microscope (Figure 1A,B Supplementary Figure S4). We also observed 1-2 UvrD foci per cell, of which 67 ± 7% (±SEM) were colocalised with DnaQ foci and 84 ± 5% of DnaQ foci were colocalised with UvrD (Figure 1B and C). We calculated the probability of random overlap between these foci, by modelling the nearest-

133 neighbour foci separation as a Poisson distribution (64), to be 20%. To confirm that
134 colocalisation between DnaQ and UvrD was not just a function of the nucleoid
135 association of UvrD, we performed Slimfield imaging of Heat-stable nucleoid-
136 structuring protein (H-NS) tagged with GFP dual labelled with DnaQ-mCherry. H-NS
137 associates with the nucleoid but not specifically with the fork. We found similar
138 numbers of H-NS foci to UvrD foci (Supplementary Figure S5) but only 38±4% DnaQ
139 foci were colocalised with H-NS implying that, similarly to the Rep helicase (13), UvrD
140 is present at the majority of replication forks.
141
142 **UvrD foci are tetrameric assemblies in live bacteria**
143

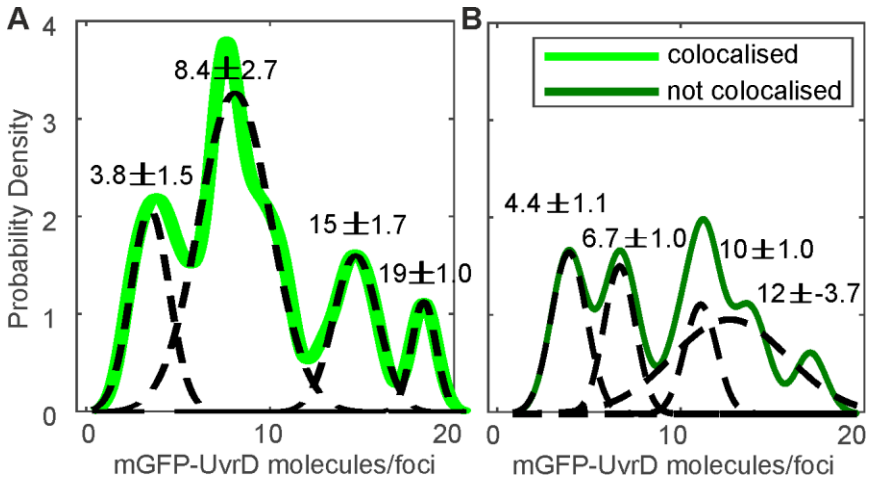

144
145 **Figure 2 UvrD stoichiometry.** The distribution of UvrD foci stoichiometry rendered as a
146 kernel density estimate for foci colocalised (A) and not colocalised (B) with DnaQ foci.
147 Distributions were fitted with multiple Gaussian peaks (black dotted lines) with the peak value
148 ± error determined by the half width at half maximum indicated above each peak
149
150 Slimfield also enabled the stoichiometry of these foci to be determined by utilizing a
151 method involving stepwise photobleaching analysis (60). Here, we determined the
152 brightness of a single-molecule of mGFP or mCherry fluorescent protein under our
153 Slimfield imaging conditions (Supplementary Figure S7), and used these values to
154 normalize the initial brightness of all tracked foci as an estimate for the stoichiometry
155 in terms of number of fluorescently labelled molecules present. We found that DnaQ
156 had the same range of 2-6 molecules per focus (Supplementary Figure S8) as we
157 have found previously, corresponding to 2-3 polymerases per fork (13, 60). The
158 distribution of the stoichiometry of UvrD foci which are colocalised with DnaQ had a
159 distinct lowest-order peak corresponding to approximately four molecules, with

160 subsequent peaks at multiples of four (Figure 2A). UvrD foci that are not colocalised
161 with DnaQ also contained a distinct lowest-order peak at four, but subsequent peaks
162 were less clearly tetrameric.
163 Although we utilised a definitive monomeric variant of GFP which contained an A206K
164 mutation to inhibit dimerization (65), we did not want to dismiss possible non-
165 physiological influences of fluorescent protein labelling of UvrD in its self-assembly
166 process. Using Size Exclusion Chromatography Multi-Angle Laser Light Scattering
167 (SEC-MALLS) we found qualitatively that the majority of UvrD runs off in a monomeric
168 fraction for both purified wild type UvrD and for the labelled construct mGFP-UvrD.
169 However, SEC-MALLS has known limitations in differentiating between monomeric
170 and oligomeric fractions due to non-specific binding to the SEC resin (depending on
171 buffering conditions), resulting in proteins eluting later than expected and co-elution of
172 monomeric species and higher mass oligomers. In addition, there are sensitivity
173 difficulties for detecting components present in relatively small quantities.
174 To overcome these limitations, we performed high-precision high-sensitivity Slimfield
175 fluorescence microscopy of purified mGFP-UvrD conjugated to a glass coverslip via
176 anti-GFP antibody (66) enabling detection of fluorescent foci bound to the surface with
177 single molecule sensitivity. Slimfield images exhibited between ~10-20 surface-bound
178 foci per field of view (Supplementary Figure S9A), whose 200-300 nm width (half width
179 at half maximum, HWHM) was comparable to that determined for single purified GFP
180 molecules. We measured the fluorescence brightness of each focus using the same
181 automated single-particle tracking software as for Slimfield experiments *in vivo*
182 (Supplementary Figure S9B), whose tracks photobleached in a stepwise manner
183 consistent with the presence of just a single GFP molecule. The amplitude of the
184 probability distribution function of foci brightness values (Supplementary Figure S9B)
185 indicated that the proportion of dimers (corresponding to a brightness of approximately
186 twice the modal value) is ~3% that of the corresponding value for monomers. Although
187 it is not possible to entirely exclude non-physiological effects of any fluorescent protein
188 on the cellular activities of a tagged protein, the finding from this single-molecule assay
189 shows that the proportion of monomeric mGFP-UvrD is substantially higher than
190 dimeric mGFP-UvrD and so, if there is an influence of mGFP on the self-assembly
191 process of UvrD, it is unlikely to be a dominant factor.
192 At higher concentrations, UvrD has been observed to exist in a monomer-dimer-
193 tetramer equilibrium *in vitro* (57). DNA unwinding experiments *in vitro* suggest UvrD

194 must function as at least a dimer (67) or a trimer (68), however the oligomeric state of
195 functional UvrD is disputed (reviewed in (69)). Our results are consistent with UvrD
196 existing predominantly as a tetramer or a dimer of dimers, with multiple tetramers or
197 dimer-dimers sometimes present at forks. It should be noted that we often observe
198 only a single DnaQ focus corresponding to two replication forks which are separated
199 by less than the diffraction limit of our microscope (Supplementary Figure S8) such
200 that some multiple tetrameric UvrD foci correspond to two replication forks. The less
201 distinct peaks in the UvrD foci that are not colocalised with DnaQ may indicate that
202 other UvrD species (monomers, dimers or trimers) are also present.
203 We were also able to determine the total cell copy number of UvrD using a method
204 which determined the total contribution of mGFP-UvrD fluorescence to the observed
205 intensity in whole cells (70). We found approximately 800 molecules of UvrD per cell
206 (Supplementary Figure S10), similar to that which we reported previously for Rep (13).
207 This is a much lower level of UvrD than was reported using transcription rate
208 measurements (71) or high-throughput proteomics (72) but is comparable to recent
209 estimates using ribosome profiling (73).
210
211 **There is no obvious interaction partner for UvrD at the fork**
212 Our earlier findings concerning the accessory helicase Rep indicated that
213 colocalisation with the fork and recruitment to the replisome were mediated by specific
214 interaction with the replicative helicase DnaB (74), with Rep and DnaB both exhibiting
215 hexameric stoichiometry (13, 60). We sought to determine whether UvrD is also
216 recruited by interacting with a specific replisome component using SPR on purified
217 UvrD and each replisome component (Supplementary Figure S11). UvrD under
218 conditions consistent with predominantly monomeric UvrD (Supplementary Figure S9)
219 exhibited no direct interaction with primase, SSB, β sliding clamp, the DNA
220 polymerase III αε, χψ or γ complexes; or θ, δ, δ′, χ, and γ subunits (12). We did initially
221 identify a putative weak UvrD-Tau interaction. However, as a control we also tested
222 Rep, and found this also interacted with Tau to a similar extent, and with ~100x lower
223 affinity than UvrD with known interaction partner UvrB (Supplementary Figure S8). We
224 therefore conclude that the Tau interaction with UvrD is likely to be non-specific and
225 that, unlike Rep, UvrD does not have an obvious, direct interaction partner at the
226 replisome, at least from the suite of replisome proteins tested. Since our findings

227 suggest that UvrD may exist as as a tetramer at the replisome, it is also unlikely to be
228 recruited by Rep, which has shown putative interaction (75).
229
230 **The presence of UvrD at the fork is mediated by specific replication blocks**

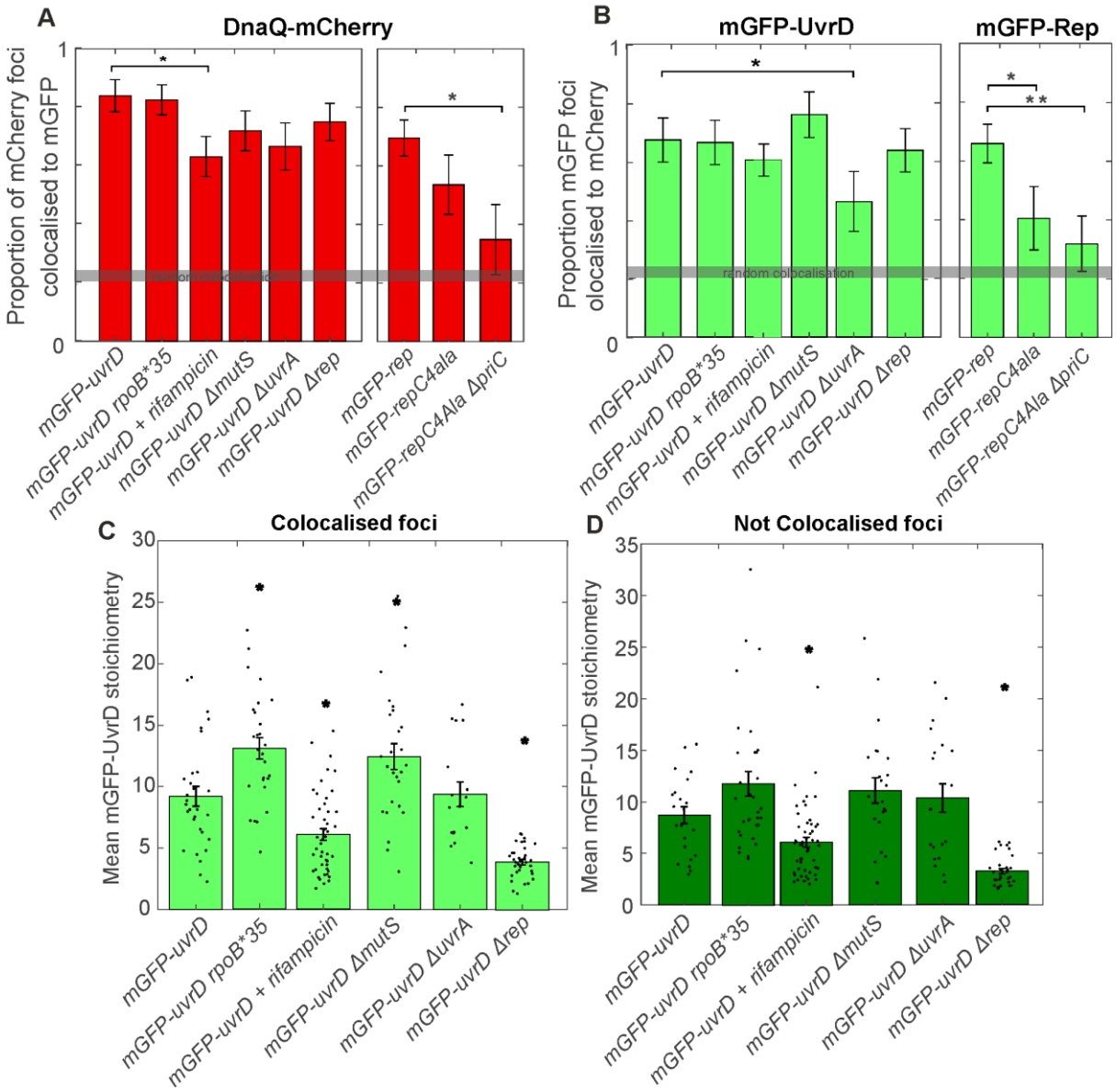

231
232 **Figure 3: UvrD perturbations**. A. and B. The mean proportion of colocalised DnaQ and
233 UvrD or Rep foci per cell respectively. Error bars represent standard error in the mean and
234 statistical significance by Brunner-Munzel and Student's t-test $p<0.05$ indicated by *. Gray
235 bar indicates levels of predicted random colocalisation. C. and D. Jitter plots of colocalised
236 and not colocalised UvrD stoichiometry respectively. Bars show mean UvrD stoichiometry
237 with error bars showing the standard error in the mean and statistical significance by
238 Brunner-Munzel and Student's t-tests $p<0.05$ indicated by *. N=30 cells.
239
240

241 Since our SPR observations indicated that UvrD most likely does not interact directly
242 and specifically with any core replisome protein, we hypothesized that the association
243 of UvrD with the replication fork might be dependent on its activity in resolving
244 nucleoprotein blocks. To test this premise, we systematically impaired key DNA
245 replication repair processes in which UvrD is implicated, as well as perturbing RNAP
246 replicative blocks by disruption of transcription through both genetic mutation and
247 antibiotic inhibition (Figure 3). We investigated how these perturbations altered fork
248 association through levels of UvrD colocalisation with DnaQ. As a control, we
249 compared these to levels of Rep colocalisation with DnaQ which can be abrogated
250 down to random levels of colocalisation, indicating no interaction with the fork, by
251 mutations which stop Rep interacting with DnaB and PriC (Figure 3A). We perturbed
252 UvrD's activity in resolving DNA damage at replication blocks by deleting *mutS* or
253 *uvrA*, rendering the strains defective in UvrD-associated mismatch repair or nucleotide
254 excision repair respectively (43, 76). We reduced the need for UvrD to remove
255 transcriptional blocks to replication (49) by introducing the *rpoB*35* mutation, which
256 destabilizes open complexes formed during initiation of transcription (77, 78); and by
257 using the antibiotic rifampicin, which blocks elongation of RNA transcripts (79). All of
258 these strains were healthy under normal growth conditions (Supplementary Figure S1,
259 Table S4) and displayed the same phenotype for DnaQ foci number and stoichiometry
260 within measurement error (Supplementary Figure S8).
261 For the transcriptional block perturbations, the *rpoB*35* mutant dual labelled strain
262 exhibited no difference in the proportion of colocalised DnaQ or UvrD foci (Figure 3A
263 and B). This mutant and all others tested exhibited the same predominant tetrameric
264 stoichiometry trends as wild type (Supplementary Figure S12), with clear peaks at
265 tetramer intervals in the colocalised stoichiometry distribution and less clear but still
266 largely tetrameric intervals in the stoichiometry distribution for UvrD foci that are not
267 colocalised with DnaQ. This provides further evidence for tetrameric UvrD assemblies
268 *in vivo*. We compared the mean stoichiometry for each mutant to that of wild type
269 (Figure 3C and D). Unexpectedly, the *rpoB*35* mutant produced a slight but
270 statistically significant increase in mean colocalised stoichiometry, corresponding to
271 approximately one extra UvrD tetramer at the replication fork (Figure 3C). This finding
272 may indicate the level of instability conferred by this mutation has multiple downstream
273 effects that alter UvrD localisation significantly at the fork. Alternatively, it could mean
274 that *rpoB*35* does not affect the formation of the types of transcriptional block that are

275 acted upon by UvrD. Rifampicin treatment produced a clearer response, reducing the
276 number of DnaQ foci colocalised with UvrD by ~20% (Figure 3A) and the mean
277 stoichiometry of colocalised and not colocalised UvrD foci by around one UvrD
278 tetramer (Figure 3C and D). Single-molecule observations of RNAP have shown it to
279 be significantly more mobile under rifampicin treatment (80), implying fewer RNAPs
280 bound to DNA and fewer blocks to replication. Our rifampicin treatment results are
281 consistent with fewer transcriptional blocks to replication reducing the amount of UvrD
282 recruited to the replisome and support the hypothesis that UvrD is recruited by these
283 replicative blocks.
284 By deleting *mutS* or *uvrA* we removed UvrD's role in mismatch repair and nucleotide
285 excision repair respectively. In the Δ*mutS* mutant we observed no change in UvrD
286 colocalisation with DnaQ, but did measure an increase the mean UvrD stoichiometry
287 colocalised with DnaQ by around one tetramer (Figure 3A). In the Δ*uvrA* mutant we
288 observed a decrease of ~25% in UvrD colocalisation with DnaQ (Figure 3B) with no
289 change in the number of UvrD foci (Supplementary Figure S8), consistent with a model
290 that UvrD association with the fork is dependent on actively resolving DNA damage
291 induced blocks to replication. The minimal response in the Δ*mutS* strain may also
292 suggest that UvrD at the fork is more involved in nucleotide excision repair than
293 mismatch repair.
294 UvrD has been shown to compensate for Rep in *rep* null mutants (12). We also tested
295 what effect this mutation would have in Slimfield *in vivo* imaging. Surprisingly, *rep*
296 deletion resulted in a steep drop in UvrD copy number (Supplementary Figure S10).
297 The degree of colocalisation between UvrD and DnaQ remained unchanged
298 compared to wild type (Figure 3A and B) but the stoichiometry of foci was reduced to
299 a single UvrD tetramer (Figure 3C and D and Supplementary Figure 11), which is
300 consistent with the observed lower copy number and availability of UvrD. The drop in
301 UvrD copy number may reflect complex regulatory shifts in response to losing such a
302 key protein in Rep, although it is interesting that even at low copy numbers, a UvrD
303 tetramer remains recruited to the fork. Double knockouts, deficient in both Rep and
304 UvrD, are lethal (12) so this minimal helicase presence must be the limit required for
305 survival.
306

307 **Dynamic association of UvrD with the fork depends on DNA repair processing**

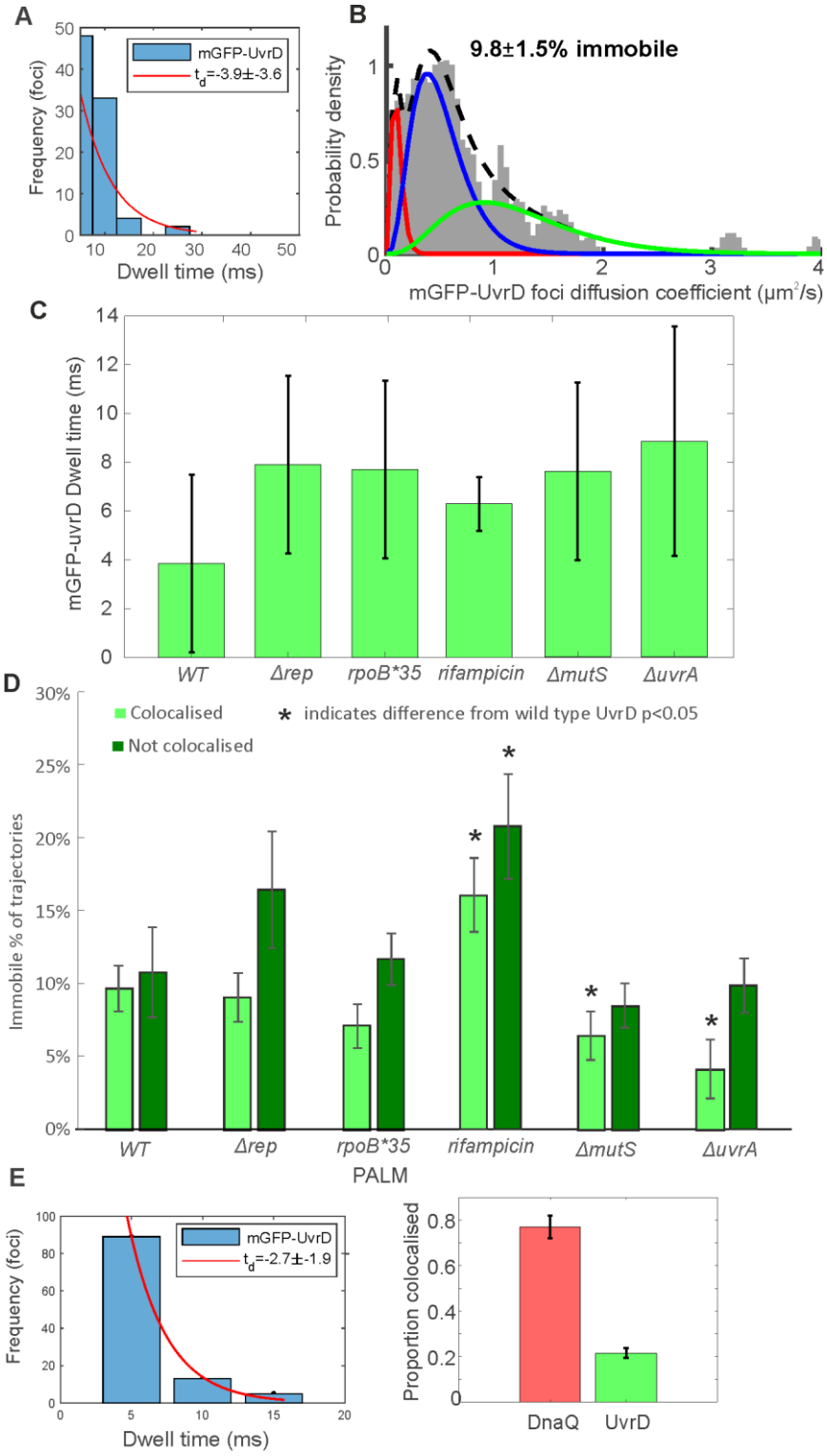

308

309 **Figure 4: UvrD dynamics.** A. Distribution of time over which UvrD and DnaQ foci were
310 colocalised (blue) fitted with an exponential (red) to yield a characteristic dwell time. B.
311 Distribution of microscopic diffusion coefficients of wild type UvrD foci (gray) fitted with a
312 three-state gamma distribution model containing a relatively immobile population with
313 $D = 0.1$ μm²/s (red), a transiently immobile population, $D = 0.5$ μm²/s (blue) and a mobile
314 population, D=1.2 μm²/s (green). C. The dwell times for each UvrD strain. Error bars represent
315 the 95% confidence intervals on the fit. D. The proportion of UvrD foci in the immobile

population for each UvrD strain colocalised or not colocalised with DnaQ foci location. Statistically significant differences $p<0.05$ from wild type indicated by *. E. PALM dwell time and colocalisation proportion of detected tracks. N=45 cells for wild type and 30 per mutant, with ~300 trajectories.

By tracking UvrD foci as a function of time using the rapid millisecond sampling enabled by Slimfield imaging, we were also able to characterize its dynamics in wild type and repair impaired cells. We measured the exposure time per frame multiplied by the number of image frames in which UvrD foci were colocalised with DnaQ foci positions and fitted the distribution of these times with a single exponential function. The corresponding time constant of this exponential fit we denote as the dwell time. We also calculated the apparent microscopic diffusion coefficient of individual foci (Figure 4 and Supplementary Figure S13). The UvrD dwell time at the fork for the wild type strain was measured to be approximately 4 ms, indicating a relatively dynamic association of UvrD at the replication fork. The apparent microscopic diffusion coefficients (D) were best fit with a three parameter Gamma model, containing a relatively immobile population with D = 0.1 $\mu m^2/s$, a transiently immobile population, D = 0.5 $\mu m^2/s$ and a mobile population, D=1.2 $\mu m^2/s$, similar to Rep (13). In wild type, we found that approximately 10% of UvrD foci were immobile, whether colocalised with the DnaQ fork location or not, with the rest of the foci split between the other two populations.

We sought to use these molecular measurements to determine the effect of perturbing UvrD-mediated DNA replication repair and block resolution on UvrD dynamics. All deletions resulted in a marginal though statistically insignificant increase in dwell time to between 6-9 ms. The Δ*rep* and *rpoB*35* mutations resulted in no change in mobility from wild type. Rifampicin treatment however, resulted in an increase in the proportion of immobile foci both at and away from the fork. This finding appears counterintuitive as rifampicin treatment results in more mobile RNAP (80), however it is unclear what effect rifampicin has on the population of RNAP molecules that remain bound to DNA. These results may suggest that such blocks provide an increased barrier to replication, decreasing mobility of UvrD as it attempts to deal with these blocks. In the Δ*mutS* and Δ*uvrA* strains, the proportion of immobile foci decreased at the fork, again consistent with the hypothesis that UvrD association with the fork is dependent on DNA damage resolution activity. One alternative explanation for these results is that UvrD is less mobile when resolving DNA damage blocks to replication and more mobile when

351 resolving transcriptional blocks, as reducing or eliminating UvrD's role in these
352 processes decreased or increased the immobile fraction in DNA repair and
353 transcription impaired cells respectively (Figure 4).
354
355 ***In vitro* biochemical experiments support the block-dependent UvrD function**
356 **model**
357 To further investigate the role of blocks in UvrD recruitment to the replisome, we
358 performed a stalled replication assay *in vitro,* which allowed us to specifically vary the
359 nucleoprotein block and the timing of UvrD recruitment i.e. before or after the
360 replisome had encountered the block. *E. coli* replisomes can be reconstituted on
361 plasmid DNA templates containing *oriC* and engineered stall sites. UvrD can be
362 included from the start of replication or added after the replisome has encountered the
363 nucleoprotein block. Blocked fork resolution was then probed by examining replication
364 products by denaturing gel electrophoresis.
365 We first used an *oriC*-containing plasmid which contained a specific RNAP stall site
366 ($P_{lacUV5\ 52C}$) to facilitate formation of a stalled transcription elongation complex via
367 nucleotide deprivation. Stalled RNAP acts as a barrier to the replisome in both head-
368 on and co-directional orientations and prevents the formation of full-length replication
369 products (1). Arresting the replisome at this RNAP block resulted in replication
370 products consisting of four truncated leading strands. The strand sizes matched those
371 expected for replisomes moving clockwise or counter-clockwise from *oriC* and
372 encountering $P_{lacUV5\ 52C}$ or the promoters within the *ColE1* plasmid origin of replication
373 (Figure 5A, lane 2 and Figure 5C) (1).
374 Inclusion of UvrD before replication initiation enabled movement of replisomes through
375 stalled RNAP and resulted in a decrease in all four truncated leading strand products
376 and a concomitant increase in production of full-length leading strands (Figure 5A,
377 lane 5 and 5E) (1). Addition of UvrD once the replisome had already encountered the
378 block gave variable results that ranged from an inhibitory to a stronger effect, although
379 differences were not statistically significant at $p<0.05$ (Figure 5A, compare lane 5 with
380 6, Figure 5E). Similar results were also obtained for Rep (Figure 5A, compare lane 3
381 with 4, Figure 5E). In the absence of replication neither Rep nor UvrD are capable of
382 pushing stalled RNAP from the $P_{lacUV5\ 52C}$ stall site (1). We found that the mGFP tag
383 does not prevent UvrD from dislodging a protein block (Supplementary Figure S14).

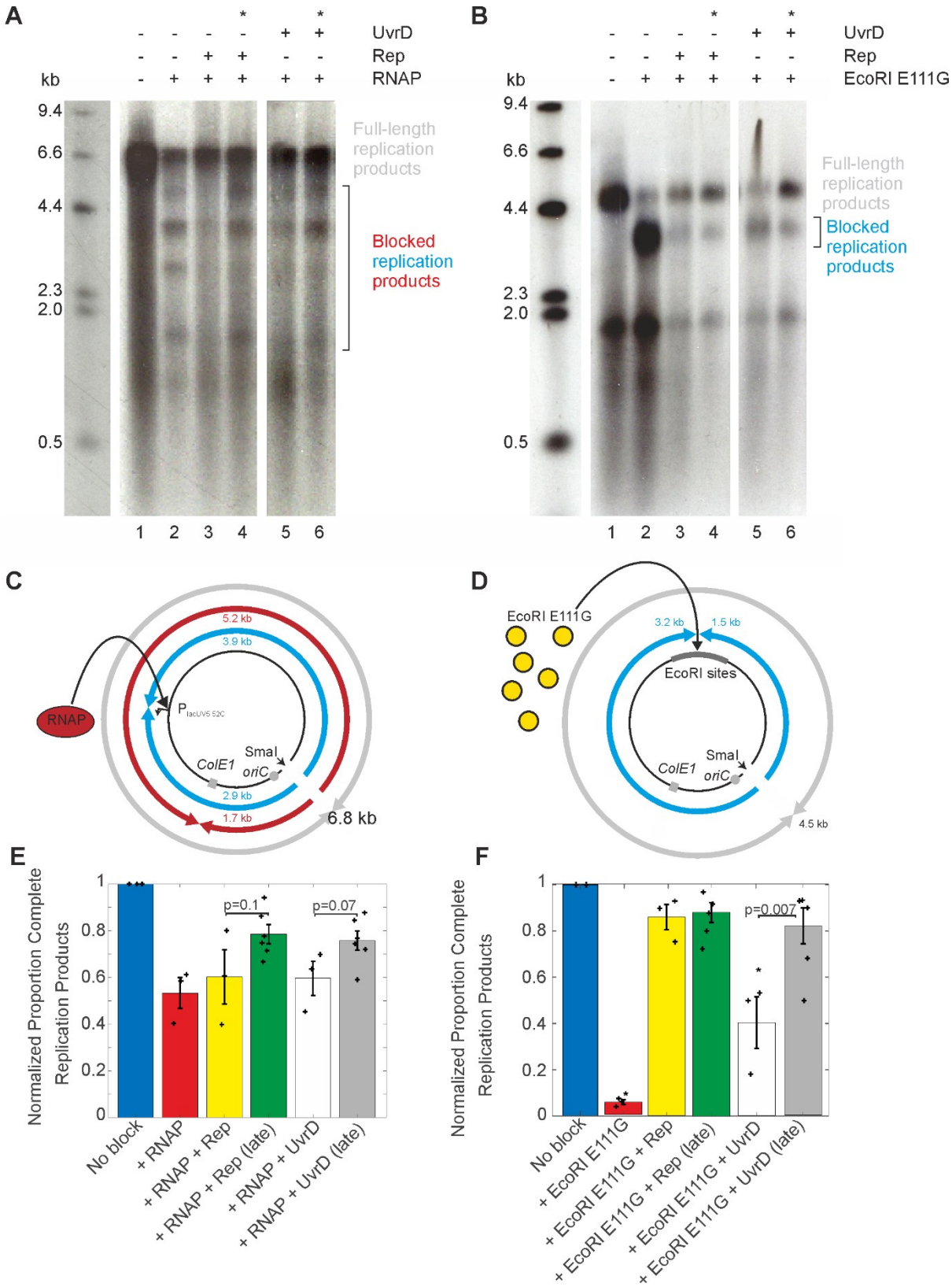

Figure 5: Helicase pre-association affects the promotion of replication fork movement through different nucleoprotein blocks A. Denaturing agarose gel of replication products formed from pPM872 (1) in the absence and presence of RNAP block, Rep and UvrD added pre- and post-collision (*) as indicated. B. Denaturing agarose gel of replication products formed from pPM594 (12) in the absence and presence of EcoRI E111G block, Rep and UvrD added pre- and post-collision (*) as indicated. Truncated leading strand products formed by

391 replisomes originating from *oriC* and colliding with RNAP (C) and EcoRI E111G (D).
392 Quantification of lanes in (A) and (B) from three technical replicates shown in (E) and (F),
393 with standard error in the mean indicated and each replicate result shown as a cross.
394

395 Since UvrD has been shown to interact with RNAP (47–49), we tested whether UvrD-
396 block pre-association is a requirement for its promotion of replication. EcoRI E111G is
397 a mutant restriction enzyme that binds to its recognition sequence but has reduced
398 cleavage activity (81). EcoRI E111G can thus act as an engineered replication fork
399 block that can be overcome by Rep or UvrD helicase activity (12). We tested whether
400 UvrD helicase could promote replication through this barrier when added before or
401 after initiation of replication on a plasmid template with an array of eight EcoRI sites
402 (Figure 5B and D). Adding UvrD post-collision did not impede its promotion of
403 replication; in fact, the resolution of these collisions appeared to be more efficient
404 because the proportion of full-length replication products increased (Figure 5B,
405 compare lane 5 and 6, 5F). Quantification of full-length replication products as a
406 proportion of reaction products showed that late UvrD addition increased full-length
407 replication products to 84% (n=6) from 41% (n=3) when UvrD is present before fork
408 collision. This contrasts with the RNAP block results where the UvrD-RNAP interaction
409 (47–50) might be responsible for localising UvrD to the block and facilitating resolution,
410 resulting in no difference when present pre- or post-collision. Similarly, Rep associates
411 directly with the replication fork, also resulting in no difference when present pre- or
412 post-collision, for both blocks. These results suggest that UvrD might recognize stalled
413 replication forks at nucleoprotein blocks using a different mechanism than Rep.
414 Combining these data with the lack of a specific replisome partner and reductions in
415 colocalisation between UvrD and DnaQ fork marker when replication blocks are
416 perturbed *in vivo*, leads us to propose that UvrD is present at the replication fork due
417 to the high frequency of different types of blocks to replication.
418

419 **DISCUSSION**

420 Here, we show that the majority of replisomes are associated with UvrD; but unlike the
421 established Rep association, UvrD has no interaction partner in the replisome. UvrD
422 instead associates with the replisome through the frequent blocks to replication
423 encountered by the fork. Similarly to Rep, *in vitro* evidence suggests UvrD functions
424 poorly as a helicase when monomeric (82). We showed previously that functional Rep
425 foci were hexameric *in vivo* but that this oligomerisation is due to interactions with

426 hexameric DnaB (13). Again, UvrD functions differently and appears to self-associate
427 into tetramers, as evidenced here by tetramer periodicity at and away from the fork
428 (Figure 2 and Supplementary Figure 11) and previous ultracentrifugation experiments
429 *in vitro* (57). It is possible that UvrD may not have evolved to fulfil exactly the same
430 function as Rep. It is common in many enzyme-catalysed reactions that if one enzyme
431 is depleted then another will be available to take its place, but with a reduced catalytic
432 efficiency (83). On initial inspection, this might appear to be the case for Rep and
433 UvrD, in light of the lower efficiency of block resolution for UvrD compared to Rep,
434 noting that deletion of Rep has a profound impact on replication whereas lack of UvrD
435 does not (84). However, we have shown that Rep and UvrD do have different modes
436 of recruitment at a replication block. These differing mechanisms of replication
437 promotion may suggest a model in which these accessory helicases have evolved to
438 fulfil the same overall function (i.e. that of resolving a block to DNA replication) but in
439 different ways. Even with different block removal efficiency, such redundancy may
440 confer an increased level of robustness, helping to ensure that the vital process of
441 DNA replication is carried out correctly by the cell.
442 We used single-molecule microscopy to show that a high proportion of forks, 80%, are
443 associated with UvrD *in vivo.* Although the raw imaging data of our Slimfield
444 microscopy is still subject to the optical resolution; the localization tracking algorithms
445 applied can pinpoint fluorescently labelled UvrD to approximately 40 nm lateral
446 precision, smaller than the 50 nm diameter of the replisome machinery itself (60) and
447 equivalent to ~100 bp DNA. Thus, our measurements for colocalisation between UvrD
448 and DnaQ are likely to be good indicators of a real interaction between the replication
449 fork and UvrD. Importantly, the degree of colocalisation we observed is much higher
450 than expectations of random overlap of the optical images of DnaQ-mCherry and
451 mGFP-UvrD.

452 Through SPR, however, we could not find any obvious, direct interaction partners at
453 the replisome apart from Tau. As a control, we tested Tau's interaction with a Rep
454 helicase, and also found a positive interaction. Thus, we conclude that the interaction
455 of UvrD with Tau is most likely to be non-specific and UvrD recruitment to the
456 replisome is mediated by blocks, rather than an interaction partner at the replisome.
457 However, we cannot know the oligomeric state of UvrD on the SPR chip and UvrD's
458 tetrameric form may affect its interactions with replisome components.

459 We probed UvrD's function at the replication fork by perturbing its known DNA repair
460 processing functions, specifically by knocking out *mutS* and *uvrA*, thus blocking
461 mismatch and nucleotide excision repair respectively. We also introduced a mutant
462 RNAP with *rpoB*35* and treated the wild type with rifampicin to reduce the occurrence
463 of transcriptional blocks to translocating replication machinery. Deleting *uvrA* and
464 rifampicin treatment produced clear results, reduced fork colocalization, but deleting
465 *mutS* and introducing the *rpoB*35* mutation did not. However, these latter
466 perturbations did result in an identical phenotype of one extra UvrD tetramer per fork.
467 The *rpoB*35* mutation improves cell viability to increased DNA lesions (77). This
468 intriguing link between mutations requires further study, possibly of these dual labelled
469 strains in response to increased DNA lesions. These data support the hypothesis that
470 UvrD is recruited to the replisome by replicative blocks. This is substantiated by the
471 reduced frequency of colocalization observed when mismatch repair and nucleotide
472 excision repair pathways involving UvrD are disrupted. RNA polymerases are the most
473 frequently encountered barrier to replication and we also see a reduction in
474 colocalization when RNA polymerases are removed by the antibiotic.
475 The only function of UvrD we did not probe directly here was its role in RecA-mediated
476 recruitment. We believe the results from a *recA* knockdown would be difficult to
477 interpret due to its pleiotropic effects. RecA is the principal recombinase and induces
478 the complex SOS response resulting in the induction of UvrD expression (85, 86).
479 Furthermore, UvrD removes RecA from RecA-DNA complexes, thus functioning as an
480 antirecombinase (87–89). Dissecting these functions of UvrD from other effects that a
481 *recA* mutation may have on the cell would be difficult. Applying the perturbations in
482 combination, i.e. double knockdowns or knockdowns plus rifampicin, would likely lead
483 to confusing results since too many deleterious perturbations may be lethal or change
484 normal cell function too radically to be biologically relevant in the intended way.
485 For the suite of mutant strains investigated we found small but significant changes in
486 colocalisation of UvrD with the replication fork, implying that UvrD is recruited to the
487 replication fork by the frequent blocks to replication it encounters. For example, the
488 UvrD-RNAP interaction could localise UvrD to the vicinity of active transcription
489 machinery (50). Since RNA polymerase is the most common replication block, a
490 secondary consequence would be UvrD-fork colocalisation. This is in contrast to the
491 Rep accessory helicase which has a specific interaction partner in the replisome of
492 the replicative helicase DnaB (74). Recent biochemical findings *in vitro* show that

493 blocks to replication occur very frequently (1)(19)(90), potentially accounting for our
494 finding that UvrD colocalises with the fork more frequently than Rep, despite Rep
495 having a specific interaction partner at the fork.
496 We have shown that replication forks stalled at transcriptional blocks can be rescued
497 by addition of UvrD, prior to or post-stalling. If UvrD is to help perform this function
498 then it must be present during the resolution of collision between the replication and
499 transcription machinery, however, our estimate for dwell time at the fork of just a few
500 milliseconds (compared to seconds for DnaQ (61)) suggests a non-negligible
501 dissociation constant; UvrD is not processive *per se* but rather undergoes rapid
502 turnover at the fork such that there is a high likelihood for UvrD being present at any
503 given time, but not necessarily the same set of molecules. Interestingly we observed
504 a similar dwell time for Rep (13), despite it having a clear association partner in DnaB
505 at the fork. However, using a defective restriction enzyme EcoRI E111G block
506 produced a different effect, with late UvrD addition improving block resolution. This
507 restriction enzyme block is artificial and less biologically relevant but may indicate that
508 the known specific UvrD interaction with RNAP is important. Improved replication
509 resolution with late addition of UvrD is intriguing, implying increased affinity for or
510 activity at pre-stalled replication forks compared to UvrD being present as the fork
511 stalls. Complete understanding requires further study of replication block resolution in
512 different conditions.

513 Our findings support a model in which UvrD diffuses and transiently interacts with DNA
514 at random or through specific interactions such as with RNAP or a specific
515 conformation of the blocked replication fork. At the DNA, UvrD is predominantly
516 tetrameric, either pre-assembling in solution or on the DNA itself. The frequent
517 sampling leads to UvrD often being in the vicinity of the replisome, allowing UvrD to
518 resolve the frequent blocks to replication. It is also possible that certain barriers to
519 replication may be harder for Rep to resolve, and such barriers can possibly be more
520 efficiently removed by UvrD, however, it is still likely to be the case that they do not
521 directly challenge the ability of the cell to replicate the genome in light of *uvrD* deletion
522 still resulting in viable cells. Indeed, UvrD shares a high degree of structural similarity
523 with Rep, although the two proteins differ significantly in their amino acid sequences
524 (31, 91). While Rep is recruited to the fork through specific interactions with DnaB, no
525 such interaction could be identified for UvrD. Stochastic impairment of the ability of

526 Rep to interact with DnaB may necessitate block processing at the fork by UvrD. In
527 summary, our results highlight the contribution of UvrD action to facilitating accurate
528 genome duplication at active replisomes.

529 **Acknowledgments**

530 We thank Maria Chechik for help with mGFP-UvrD purification. We thank Prof. Nigel
531 Savery (University of Bristol) for the gift of the pETDuet-UvrD overexpression plasmid.
532 We thank the Molecular Interactions Laboratory in the Bioscience Technology Facility
533 at the University of York for technical assistance and support. Supported by BBSRC
534 via grants BB/N006453/1 (M.L., P.M.), BB/R001235/1 (M.L.,P.M.), BB/N014863/1
535 (M.H.).

536

537 **Author Contributions**

538 Conceptualization: AJMW, AS, PMG, MH, MCL
539 Methodology: AJMW, AS, JALH, AL, CG, PMG, MH, MCL
540 Software: AJMW
541 Investigation: AJMW, AS, JALH, APD, AL, CG, MH
542 Visualization: AJMW, AS, MH
543 Supervision: AJMW, AS, MH, PMG, MCL
544 Writing—original draft: AJMW, AS, MH, MCL
545 Writing—review & editing: AJMW, AS, JALH, AL, PMG, MH, MCL
546

547 **Declaration of interests**

548 The authors declare no competing interests.
549

550 **MATERIALS AND METHODS**

551 **Strain construction**

552 All strains used in this study (listed in full in SI Table S1, with associated plasmids
553 and primers in SI Tables S2 and S3) are derivatives of the laboratory wild type strain
554 TB28. Tagging of *dnaQ-mCherry-<kan>* (C-terminally labelled) is described in (13).
555 *mGFP-uvrD-<kan>* (N-terminally labelled) was amplified from plasmid pAS79 (*uvrD*$^{+}$)

556 with primers oAS145 and oJGB383 having 50 bp homology to either end of the
557 native *uvrD* locus. The resulting PCR product had homology either side such that
558 recombination with the chromosome would result in integration of the PCR product at
559 the native locus under the control of the native promoter. Prior to integration, all PCR
560 products were treated with DpnI, gel purified, and introduced by electroporation into
561 cells expressing the lambda Red genes from the plasmid pKD46 (55). The
562 recombinants were selected for kanamycin resistance and screened for ampicillin
563 sensitivity. The colonies obtained were verified for integration by PCR and
564 sequencing. The *uvrD* recombinants were verified by PCR amplification using
565 primers oPM319 and oPM320, and sequencing using the primers oJGB417,
566 oJGB418, oPM407, oPM409, oPM411, and oMKG71. Where required, the
567 kanamycin resistance gene was removed by expressing Flp recombinase from the
568 plasmid pCP20 (92) to generate kanamycin sensitive strains carrying the fluorescent
569 protein (FP) fusions. Dual labelled strains were created by introducing the kanamycin
570 tagged FP alleles by standard P1 mediated transduction into single labelled strains
571 carrying the required FP allele after removing the linked kanamycin marker.

572 **Determination of cell doubling time**

573 *E. coli* strains were grown overnight in LB medium at 37°C at 200 rpm shaking. The
574 saturated overnight cultures were diluted 100-fold into fresh LB or washed once with
575 1X 56 salts and diluted 100-fold in fresh 1X 56 salts with 0.2% glucose as the carbon
576 source. Aliquots of 100 µl each of the diluted cultures in fresh media were pipetted
577 into individual wells of 96 well clear flat bottom sterile microplates (Corning). The
578 microplates containing the diluted cultures were incubated in a BMG LABTECH
579 SPECTROstar Nano microplate reader at 37°C and the optical density (A_{600}) values
580 were recorded at defined time intervals. The time taken for the optical density values
581 to increase 2-fold during the exponential growth phase of the culture was taken as
582 the cell doubling time (SI Table S4, Supplementary Figure S1).

583 **Protein Overexpression and Purification**

584 *mGFP-uvrD* was excised from pAS79 using XhoI and SalI and ligated into pET14b
585 cut with XhoI, creating pAS152 encoding N-terminal histidine-tagged mGFP-UvrD.
586 pAS152 was used to overexpress the mGFP-UvrD fusion in Rosetta™
587 2(DE3)/pLysS. The cells were grown in LB medium containing 100 µg/ml ampicillin

588 and 30 µg/ml chloramphenicol at 37ºC and 220 rpm to OD_{600} ~ 0.7. The cultures
589 were then equilibrated to room temperature and overexpression was induced by
590 adding 1 mM IPTG and incubating at 16ºC for 24 hours. Cells from the expressed
591 culture were collected by centrifugation at 4ºC and frozen at -80ºC. The cells were
592 later thawed on ice and resuspended in buffer A (20 mM Tris-Cl pH 8.3, 500 mM
593 NaCl, 5 mM imidazole, 10% glycerol) along with 0.1 mg/ml lysozyme, 1 mM AEBSF,
594 0.7 µg/ml pepstatin, 0.5 µg/ml leupeptin, 2.5 µg/ml DNase I and 20 µg/ml RNase A
595 and incubated on ice for 30 minutes. Brij-58 was then added to a final concentration
596 of 0.1% v/v and incubated on ice for another 20 minutes. The suspension was
597 sonicated and then clarified by centrifugation at 18,000 rpm for 60 minutes at 4ºC in
598 an SS-34 rotor to remove debris. The lysate containing mGFP-UvrD was applied to a
599 5 ml His-trap FF crude column (GE healthcare) and the protein was purified by
600 chromatography on an imidazole gradient in buffer A. Peak fractions were collected
601 and concentrated using a Vivaspin 500 concentrator (30 kDa MWCO) (Sartorius).
602 Samples were then aliquoted and flash frozen in liquid nitrogen before storage at -
603 80ºC. Protein concentration was determined by Bradford's assay.

604 UvrD was purified as previously described (55). Briefly UvrD was overexpressed in
605 BL21-AI from a pETDuet vector, via induction by IPTG and arabinose. UvrD was
606 purified from the soluble cell extract after lysis through the use of affinity (heparin
607 agarose), anion exchange (Q-sepharose), and gel filtration chromatography. Pure
608 UvrD was then stored at -80ºC after dialysis into storage buffer or used immediately
609 in Size Exclusion Chromatography - Multi-Angle Laser Light Scattering (SEC-
610 MALLS) analysis or subsequently diluted to 1 nM for single-molecule *in vitro*
611 experimentation.

612 Biotinylated UvrD and Rep were purified as previously described (12). Briefly, the
613 proteins were overexpressed in a BL21 (DE3) containing pBirAcm, encoding a biotin
614 ligase via induction by IPTG and the addition of biotin to the growth media. The
615 biotinylated proteins were then purified from the soluble cell extracts by ammonium
616 sulphate precipitation, and affinity chromatography (softlink avidin and heparin
617 agarose). Pure proteins were then dialysed into storage buffer overnight and stored
618 at -80°C

619 **Helicase assay**

620 Assays for unwinding of streptavidin-bound forks were performed using a substrate
621 made by annealing oligonucleotides oPM187B20 (5' end labelled with ^{32}P) and
622 oPM188B34. Reactions were performed in 10 µL volumes containing 40 mM HEPES
623 (pH 8); 10 mM DTT; 10 mM magnesium acetate; 2 mM ATP; 0.1 mg ml^{-1} BSA and
624 1 nM forked DNA substrate. Reactions were carried out as described earlier (13, 93).
625 Briefly, the reaction mixture was pre-incubated at 37°C for five minutes with or
626 without 1 µM streptavidin (Sigma-Aldrich), to which helicase (as indicated) and biotin
627 (Sigma-Aldrich) were added to 100 µM (acting as a trap for free streptavidin) and
628 incubated at 37°C for another 10 minutes. Reactions were stopped by addition of 2.5
629 µl of 2.5% SDS, 200 mM EDTA and 10 mg ml^{-1} of proteinase K. Reactions were then
630 analysed by non-denaturing gel electrophoresis on 10% polyacrylamide TBE gels.
631 The quantification of the unwinding and displacement of streptavidin from the fork
632 was carried out as described in (94).

633 **Preparation of cells for microscopy**

634 Cells were grown overnight in LB to saturation. The overnight cultures were
635 inoculated the next day at 1:1000 dilution in 1X 56 salts supplemented with 0.2%
636 glucose as the carbon source. The dilutions were then grown at 30°C to mid-log
637 phase.

638 **Rifampicin treatment**

639 Cells prepared for microscopy were treated with rifampicin at a final concentration of
640 50 µg/mL for 30 minutes at 30°C.

641 **Microscopy and image analysis**

642 Imaging was performed on a bespoke dual-colour single-molecule microscope (13).
643 Excitation from Obis 488 nm and 561 nm wavelength 50mW lasers (run at 20 mW)
644 was reduced to 10 µm at full width half maximum field in the sample plane producing
645 Slimfield illumination (58) producing a mean excitation intensity of ~0.25 mW/μm^2.
646 Lasers were digitally modulated to 5 ms period to produce alternating laser excitation
647 using National Instruments dynamic I/O module NI 9402. Excitation was coupled into
648 a Zeiss microscope body with the sample mounted on a Mad City Labs nanostage.
649 Images were magnified to 80nm/pixel and imaged using an Andor Ixon 128 emCCD
650 camera. Colour channels were split red/green using a bespoke colour splitter

651 consisting of a dual-pass green/red dichroic mirror centred at long-pass wavelength
652 560 nm and emission filters with 25 nm bandwidths centred at 542 nm and 594 nm.

653 Cells were imaged on agarose pads suffused with minimal media as described
654 previously (95). Foci were detected and tracked using previously described bespoke
655 MATLAB software (96). In brief, bright candidate foci were detected in each frame by
656 image transformation and thresholding based on Otsu's method. A 17x17 pixel
657 region of interest (ROI) is drawn around each candidate to define the local
658 background, while a radius 5 circle is drawn in the center (the foreground) and
659 subjected to iterative Gaussian masking (66). Foci were accepted if their signal to
660 noise ratio was above 0.4, defined as the mean intensity inside the foreground
661 divided by the standard deviation of the local background. Foci in successive frames
662 were linked together into trajectories based on nearest distance, provided it was < 5
663 pixels. Linked foci were accepted as "tracks" nominally if they persist for at least 4
664 consecutive image frames.

665 Characteristic intensity of mGFP or mCherry was determined from the distribution of
666 foci intensity values towards the end of the photobleach confirmed by overtracking
667 foci beyond their bleaching and applying an edge-preserving filter (97, 98) to the raw
668 intensity data to generate individual steps of the characteristic intensity, due to
669 photobleaching (Supplementary Figure S7). This intensity was used to determine the
670 stoichiometry of foci by fitting the first 3 intensity points with a straight line and
671 dividing the intercept by this characteristic intensity. The number of peaks in the
672 Gaussian fits to UvrD was set by running a peak fitting algorithm over the wild type
673 distribution. This number of Gaussians was then used for mutant distributions unless
674 two or more of the Gaussians converged on the same/similar peak value, in which
675 case they were removed. For DnaQ, two peaks were fit as used previously (60).

676 GFP and mCherry images were aligned based on the peak of the 2D cross
677 correlation between their respective brightfield images. Colocalisation between foci
678 and the probability of random colocalisation was determined as described previously
679 (64, 99).

680 The microscopic apparent diffusion coefficients (*D*) were determined by fitting a
681 straight line to the first three mean squared displacements (MSD) values constrained
682 through the equivalent localization precision MSD as determined from the intensity

683 (70, 100). *D* distributions were fit by three Gamma distributions as described
684 previously (101–103). Dwell time was calculated as the number of frames that each
685 trajectory was colocalised with the fork position, as determined by the DnaQ foci
686 detected at time zero.

687 **Single-molecule *in vitro* imaging**

688 10 µg/mL mouse anti-GFP (Roche. Cat no. 11814460001) in PBS was incubated on
689 a tunnel slide for 5 min at room temperature, before washing with 100 µL of imaging
690 buffer (20 mM Tris pH 7.8, 5 mM $MgCl_2$, 1 mM DTT). 1 nM of purified mGFP-UvrD in
691 imaging buffer was then flowed onto the slide and incubated at room temperature for
692 5 min before washing with 100 µL of imaging buffer. The ends of the channel were
693 then sealed for imaging. We used a similar single-molecule fluorescence microscope
694 design (99) which enabled Slimfield microscopy as for the live cell imaging in order
695 to image the antibody immobilised mGFP-UvrD.

696 **SEC-MALLS**

697 Size Exclusion Chromatography – Multi-Angle Laser Light Scattering (SEC-MALLS)
698 experiments used Wyatt HELEOS-II multi-angle light scattering and rEX refractive
699 index detectors linked to a Shimadzu HPLC system (SPD-20A UV detector, LC20-
700 AD isocratic pump system, DGU-20A3 degasser and SIL-20A autosampler) with a
701 G.E. Superdex S200 10/300 column at a flow rate of 0.5 mL/min in buffer of 20 mM
702 Tris pH 8.3 (at 4degC) 1 mM EDTA, 1 mm EGTA, 1 mM DTT, 200 mM NaCl, 5%
703 glycerol buffer. Data were analysed using Wyatt Astra 7 software. MWs were
704 estimated using the Zimm fit method with degree 1. A value of 0.182 mL/g was used
705 for protein refractive index increment (dn/dc).

706 **Surface plasmon resonance (SPR)**

707 SPR was performed at 25°C on a BIAcore T200 instrument as in (12). Immobilisation
708 of *E. coli* UvrD and Rep was performed onto streptavidin-coated SA sensor chips
709 whilst the indicated concentrations of Tau and UvrB were passed over in 10 mM
710 HEPES pH 7.4, 3 mM EDTA, 150 mM NaCl, 10 mM $MgCl_2$ and 0.05% Tween 20 at
711 20 µl min^{-1}. This buffer differed from that used in the DNA replication assays to
712 minimise non-specific interactions with the surface-immobilised streptavidin.

713 **Replication assay**

714 Replication assays were carried out using pPM872 as the template for RNAP blocks
715 (1) or pPM594 (12) for EcoRI E111G blocks. Plasmid pPM872 contains $P_{lacUV5\ 52C}$, a
716 strong promoter in which the first 52 nucleotides of the transcript lack cytosine
717 residues and are then followed by four consecutive cytosines. This enables
718 transcription of $P_{lacUV5\ 52C}$ to be stalled by the omission of CTP. Assays were
719 performed in 40 mM HEPES (pH 8); 10 mM DTT; 10 mM magnesium acetate; 2 mM
720 ATP; 0.2 mM GTP, 0.2 mM UTP; 0.04 mM dNTPs; and 0.1 mg/ml BSA. Reactions
721 (15 µl) contained 2 nM plasmid template, 50 nM DNA polymerase III αεθ complex,
722 25 nM τ clamp loader complex, 160 nM DnaB and DnaC monomers, 1 µM SSB, 80
723 nM β clamp, 30 nM HU, 200 nM DnaG, 300 nM DnaA. Helicases were added as
724 indicated. Rep and UvrD used at 200 nM. *E. coli* RNAP holoenzyme from NEB (1
725 U/µl) was used at 1/3 dilution. Dilution was determined empirically to match RNAP
726 replication inhibition levels from (1). EcoRI E111G was purified as in (104) and used
727 at 200 nM. Reactions were assembled on ice and initiated by addition of DnaA and
728 incubation for 4 min at 37°C, followed by addition of 60 units SmaI (Promega) plus
729 0.4 MBq [α^{32}P] dCTP (222 TBq/mmol). Standard reactions with the helicase present
730 in the initial protein mix were carried out at 37°C for 1 minute and then terminated by
731 addition of 1 µl of 0.5 M EDTA. Delayed helicase addition was carried out by adding
732 Rep/UvrD after 1 minute and incubation for a further minute at 37°C before
733 termination with EDTA. Ethanol precipitated replication products were analysed by
734 denaturing agarose gel electrophoresis (0.7% agarose in 2 mM EDTA, 30 mM NaOH
735 for 400 volt hours, standard run was 16 hours at 25 V), phosphorimaging and
736 autoradiography. 5'-labelled HindIII- digested lambda DNA was used as a marker.
737 Gels were quantified using Quantity One® (Bio-Rad) software. Full-length plasmid
738 replication products were quantified as a proportion of summed blocked products
739 and normalised for length (for EcoRI E111G block), or total lane signal (RNAP
740 block).

741

742
743

744

745
746 **REFERENCES**
747

748 1. M. Hawkins, *et al.*, Direct removal of RNA polymerase barriers to replication by
749 accessory replicative helicases. *Nucleic Acids Res.* **47** (2019).
750 2. R. T. Pomerantz, M. O'Donnell, The replisome uses mRNA as a primer after
751 colliding with RNA polymerase. *Nature* **456**, 762–767 (2008).
752 3. H. Merrikh, C. Machón, W. H. Grainger, A. D. Grossman, P. Soultanas, Co-
753 directional replication-transcription conflicts lead to replication restart. *Nature*
754 **470**, 554–7 (2011).
755 4. A. H. Syeda, J. Atkinson, R. G. Lloyd, P. McGlynn, The balance between
756 recombination enzymes and accessory replicative helicases in facilitating
757 genome duplication. *Genes (Basel).* **7** (2016).
758 5. A. Helmrich, M. Ballarino, L. Tora, Collisions between replication and
759 transcription complexes cause common fragile site instability at the longest
760 human genes. *Mol. Cell* **44**, 966–977 (2011).
761 6. Y. Takeuchi, T. Horiuchi, T. Kobayashi, Transcription-dependent
762 recombination and the role of fork collision in yeast rDNA. *Genes Dev.* **17**,
763 1497–1506 (2003).
764 7. A. L. de Septenville, S. Duigou, H. Boubakri, B. Michel, Replication fork
765 reversal after replication-transcription collision. *PLoS Genet.* **8** (2012).
766 8. C. J. Rudolph, A. L. Upton, A. Stockum, C. A. Nieduszynski, R. G. Lloyd,
767 Avoiding chromosome pathology when replication forks collide. *Nature* **500**,
768 608–611 (2013).
769 9. B. Michel, G. Grompone, M. J. Florès, V. Bidnenko, Multiple pathways process
770 stalled replication forks. *Proc. Natl. Acad. Sci. U. S. A.* **101**, 12783–12788
771 (2004).
772 10. E. V. Mirkin, S. M. Mirkin, Mechanisms of transcription-replication collisions in
773 bacteria. *Mol. Cell. Biol.* **25**, 888–895 (2005).
774 11. P. McGlynn, N. J. Savery, M. S. Dillingham, The conflict between DNA
775 replication and transcription. *Mol. Microbiol.* **85**, 12–20 (2012).
776 12. C. P. Guy, *et al.*, Rep provides a second motor at the replisome to promote
777 duplication of protein-bound DNA. *Mol. Cell* **36**, 654–666 (2009).
778 13. A. H. Syeda, *et al.*, Single-molecule live cell imaging of Rep reveals the
779 dynamic interplay between an accessory replicative helicase and the
780 replisome. *Nucleic Acids Res.* **47**, 6287–6298 (2019).
781 14. P. McGlynn, Linking transcription with DNA repair, damage tolerance, and
782 genome duplication. *Proc. Natl. Acad. Sci. U. S. A.* **107**, 15314–15315 (2010).
783 15. D. Dutta, K. Shatalin, V. Epshtein, M. E. Gottesman, E. Nudler, Linking RNA
784 polymerase backtracking to genome instability in E. coli. *Cell* **146**, 533–543
785 (2011).
786 16. D. Duchi, *et al.*, RNA Polymerase Pausing during Initial Transcription. *Mol. Cell*
787 **63**, 939–950 (2016).
788 17. G. Ghosal, J. Chen, DNA damage tolerance: a double-edged sword guarding
789 the genome. *Transl. Cancer Res.* **2**, 107–129 (2013).
790 18. S. Hamperl, M. J. Bocek, J. C. Saldivar, T. Swigut, K. A. Cimprich,
791 Transcription-Replication Conflict Orientation Modulates R-Loop Levels and
792 Activates Distinct DNA Damage Responses. *Cell* **170**, 774-786.e19 (2017).
793 19. K. Hizume, H. Araki, Replication fork pausing at protein barriers on
794 chromosomes. *FEBS Lett.* **593**, 1449–1458 (2019).

795 20. K. K. Myka, M. E. Gottesman, DksA and DNA double-strand break repair.
796 *Curr. Genet.* **65**, 1297–1300 (2019).
797 21. K. K. Myka, *et al.*, Inhibiting translation elongation can aid genome duplication
798 in Escherichia coli. *Nucleic Acids Res.* **45**, 2571–2584 (2017).
799 22. S. M. Mangiameli, C. N. Merrikh, P. A. Wiggins, H. Merrikh, Transcription leads
800 to pervasive replisome instability in bacteria. *Elife* **6** (2017).
801 23. V. Kamarthapu, *et al.*, ppGpp couples transcription to DNA repair in E. coli.
802 *Science* **352**, 993–996 (2016).
803 24. B. J. Brewer, When polymerases collide: replication and the transcriptional
804 organization of the E. coli chromosome. *Cell* **53**, 679–686 (1988).
805 25. A. Srivatsan, A. Tehranchi, D. M. MacAlpine, J. D. Wang, Co-orientation of
806 replication and transcription preserves genome integrity. *PLoS Genet.* **6**
807 (2010).
808 26. B. Liu, B. M. Alberts, Head-on collision between a DNA replication apparatus
809 and RNA polymerase transcription complex. *Science* **267**, 1131–1137 (1995).
810 27. J. D. Wang, M. B. Berkmen, A. D. Grossman, Genome-wide coorientation of
811 replication and transcription reduces adverse effects on replication in Bacillus
812 subtilis. *Proc. Natl. Acad. Sci. U. S. A.* **104**, 5608–5613 (2007).
813 28. T. S. Sankar, B. D. Wastuwidyaningtyas, Y. Dong, S. A. Lewis, J. D. Wang,
814 The nature of mutations induced by replication–transcription collisions. *Nature*
815 **535**, 178–181 (2016).
816 29. D. Ivanova, *et al.*, Shaping the landscape of the Escherichia coli chromosome:
817 replication-transcription encounters in cells with an ectopic replication origin.
818 *Nucleic Acids Res.* **43**, 7865–7877 (2015).
819 30. A. Helmrich, M. Ballarino, E. Nudler, L. Tora, Transcription-replication
820 encounters, consequences and genomic instability. *Nat. Struct. Mol. Biol.* **20**,
821 412–418 (2013).
822 31. J. G. Brüning, J. L. Howard, P. McGlynn, Accessory replicative helicases and
823 the replication of protein-bound DNA. *J. Mol. Biol.* **426**, 3917–3928 (2014).
824 32. K. R. McDonald, *et al.*, Pfh1 Is an Accessory Replicative Helicase that
825 Interacts with the Replisome to Facilitate Fork Progression and Preserve
826 Genome Integrity. *PLoS Genet.* **12** (2016).
827 33. J. E. Sokoloski, A. G. Kozlov, R. Galletto, T. M. Lohman, Chemo-mechanical
828 pushing of proteins along single-stranded DNA. *Proc. Natl. Acad. Sci. U. S. A.*
829 **113**, 6194–6199 (2016).
830 34. G. D. Schauer, *et al.*, Replisome bypass of a protein-based R-loop block by
831 Pif1. *Proc. Natl. Acad. Sci. U. S. A.* **117**, 30354–30361 (2020).
832 35. M. K. Gupta, *et al.*, Protein-DNA complexes are the primary sources of
833 replication fork pausing in Escherichia coli. *Proc. Natl. Acad. Sci. U. S. A.* **110**,
834 7252–7257 (2013).
835 36. H. Boubakri, A. L. De Septenville, E. Viguera, B. Michel, The helicases DinG,
836 Rep and UvrD cooperate to promote replication across transcription units in
837 vivo. *EMBO J.* **29**, 145–157 (2010).
838 37. X. Liu, J. X. Seet, Y. Shi, P. R. Bianco, Rep and UvrD Antagonize One Another
839 at Stalled Replication Forks and This Is Exacerbated by SSB. *ACS Omega* **4**,
840 5180–5196 (2019).
841 38. O. Adebali, Y. Y. Chiou, J. Hu, A. Sancar, C. P. Selby, Genome-wide
842 transcription-coupled repair in Escherichia coli is mediated by the Mfd
843 translocase. *Proc. Natl. Acad. Sci. U. S. A.* **114**, E2116–E2125 (2017).
844 39. N. Kang, E. Choi, S. G. Kim, J. Hwang, Inhibitory effect of UvrD and DinG on

845 the replication of ColE1-derived plasmids in Escherichia coli. *Plasmid* **81**, 32–
846 41 (2015).
847 40. V. Epshtein, UvrD helicase: an old dog with a new trick: how one step
848 backward leads to many steps forward. *Bioessays* **37**, 12–19 (2015).
849 41. P. R. Caron, S. R. Kushner, L. Grossman, Involvement of helicase II (uvrD
850 gene product) and DNA polymerase I in excision mediated by the uvrABC
851 protein complex. *Proc. Natl. Acad. Sci. U. S. A.* **82**, 4925–4929 (1985).
852 42. V. H. B, Nucleotide excision repair in Escherichia coli. *Microbiol. Rev.* **54**, 18–
853 51 (1990).
854 43. A. L. Lu, S. Clark, P. Modrich, Methyl-directed repair of DNA base-pair
855 mismatches in vitro. *Proc. Natl. Acad. Sci. U. S. A.* **80**, 4639–4643 (1983).
856 44. S. W. Matson, A. B. Robertson, The UvrD helicase and its modulation by the
857 mismatch repair protein MutL. *Nucleic Acids Res.* **34**, 4089–4097 (2006).
858 45. L. Manelyte, *et al.*, The unstructured C-terminal extension of UvrD interacts
859 with UvrB, but is dispensable for nucleotide excision repair. *DNA Repair*
860 *(Amst).* **8**, 1300–1310 (2009).
861 46. A. B. Robertson, S. R. Pattishall, E. A. Gibbons, S. W. Matson, MutL-catalyzed
862 ATP hydrolysis is required at a post-UvrD loading step in methyl-directed
863 mismatch repair. *J. Biol. Chem.* **281**, 19949–19959 (2006).
864 47. E. J. Gwynn, *et al.*, The conserved C-terminus of the PcrA/UvrD helicase
865 interacts directly with RNA polymerase. *PLoS One* **8** (2013).
866 48. K. Sanders, *et al.*, The structure and function of an RNA polymerase
867 interaction domain in the PcrA/UvrD helicase. *Nucleic Acids Res.* **45**, 3875–
868 3887 (2017).
869 49. V. Epshtein, *et al.*, UvrD facilitates DNA repair by pulling RNA polymerase
870 backwards. *Nature* **505**, 372–377 (2014).
871 50. B. K. Bharati, *et al.*, Crucial role and mechanism of transcription-coupled DNA
872 repair in bacteria. *Nature* **604**, 152–159 (2022).
873 51. B. Martinez, B. K. Bharati, V. Epshtein, E. Nudler, Pervasive Transcription-
874 coupled DNA repair in E. coli. *Nat. Commun.* **13** (2022).
875 52. N. M. Haines, Y. I. T. Kim, A. J. Smith, N. J. Savery, Stalled transcription
876 complexes promote DNA repair at a distance. *Proc. Natl. Acad. Sci. U. S. A.*
877 **111**, 4037–4042 (2014).
878 53. A. J. Smith, N. J. Savery, Effects of the bacterial transcription-repair coupling
879 factor during transcription of DNA containing non-bulky lesions. *DNA Repair*
880 *(Amst).* **7**, 1670–1679 (2008).
881 54. A. J. Smith, N. J. Savery, RNA polymerase mutants defective in the initiation of
882 transcription-coupled DNA repair. *Nucleic Acids Res.* **33**, 755–764 (2005).
883 55. J. Atkinson, *et al.*, Stimulation of UvrD helicase by UvrAB. *J. Biol. Chem.* **284**,
884 9612–9623 (2009).
885 56. R. P. Wong, N. García-Rodríguez, N. Zilio, M. Hanulová, H. D. Ulrich,
886 Processing of DNA Polymerase-Blocking Lesions during Genome Replication
887 Is Spatially and Temporally Segregated from Replication Forks. *Mol. Cell* **77**,
888 3-16.e4 (2020).
889 57. N. K. Maluf, T. M. Lohman, Self-association equilibria of Escherichia coli UvrD
890 helicase studied by analytical ultracentrifugation. *J. Mol. Biol.* **325**, 889–912
891 (2003).
892 58. M. Plank, G. H. Wadhams, M. C. Leake, Millisecond timescale slimfield
893 imaging and automated quantification of single fluorescent protein molecules
894 for use in probing complex biological processes. *Integr. Biol.* **1**, 602–612

895 (2009).
896 59. A. Badrinarayanan, R. Reyes-Lamothe, S. Uphoff, M. C. Leake, D. J. Sherratt,
897 In vivo architecture and action of bacterial structural maintenance of
898 chromosome proteins. *Science* **338**, 528–31 (2012).
899 60. R. Reyes-Lamothe, D. J. Sherratt, M. C. Leake, Stoichiometry and architecture
900 of active DNA replication machinery in Escherichia coli. *Science* **328**, 498–501
901 (2010).
902 61. T. R. Beattie, *et al.*, Frequent exchange of the DNA polymerase during
903 bacterial chromosome replication. *Elife* **6**, e21763 (2017).
904 62. R. Reyes-Lamothe, C. Possoz, O. Danilova, D. J. Sherratt, Independent
905 positioning and action of Escherichia coli replisomes in live cells. *Cell* **133**, 90–
906 102 (2008).
907 63. A. L. Payne-Dwyer, A. H. Syeda, J. W. Shepherd, L. Frame, M. C. Leake,
908 RecA and RecB: probing complexes of DNA repair proteins with mitomycin C
909 in live Escherichia coli with single-molecule sensitivity. *bioRxiv*,
910 2021.10.04.463068 (2021).
911 64. I. Llorente-Garcia, *et al.*, Single-molecule in vivo imaging of bacterial
912 respiratory complexes indicates delocalized oxidative phosphorylation.
913 *Biochim. Biophys. Acta* **1837**, 811–24 (2014).
914 65. D. A. Zacharias, J. D. Violin, A. C. Newton, R. Y. Tsien, Partitioning of lipid-
915 modified monomeric GFPs into membrane microdomains of live cells. *Science*
916 **296**, 913–916 (2002).
917 66. M. C. Leake, *et al.*, Stoichiometry and turnover in single, functioning
918 membrane protein complexes. *Nature* **443**, 355–358 (2006).
919 67. N. K. Maluf, C. J. Fischer, T. M. Lohman, A Dimer of Escherichia coli UvrD is
920 the active form of the helicase in vitro. *J. Mol. Biol.* **325**, 913–935 (2003).
921 68. H. Yokota, Y. A. Chujo, Y. Harada, Single-molecule imaging of the oligomer
922 formation of the nonhexameric Escherichia coli UvrD helicase. *Biophys. J.* **104**,
923 924–933 (2013).
924 69. H. Yokota, Quantitative and kinetic single-molecule analysis of DNA unwinding
925 by Escherichia coli UvrD helicase. *Biophys. physicobiology* **19**, n/a (2022).
926 70. A. J. M. Wollman, M. C. Leake, Millisecond single-molecule localization
927 microscopy combined with convolution analysis and automated image
928 segmentation to determine protein concentrations in complexly structured,
929 functional cells, one cell at a time. *Faraday Discuss.* **184**, 401–24 (2015).
930 71. H. M. Arthur, P. B. Eastlake, Transcriptional control of the uvrD gene of
931 Escherichia coli. *Gene* **25**, 309–316 (1983).
932 72. Y. Taniguchi, *et al.*, Quantifying E. coli proteome and transcriptome with
933 single-molecule sensitivity in single cells. *Science* **329**, 533–8 (2010).
934 73. G. W. Li, D. Burkhardt, C. Gross, J. S. Weissman, Quantifying absolute protein
935 synthesis rates reveals principles underlying allocation of cellular resources.
936 *Cell* **157**, 624–635 (2014).
937 74. J. Atkinson, M. K. Gupta, P. McGlynn, Interaction of Rep and DnaB on DNA.
938 *Nucleic Acids Res.* **39**, 1351–1359 (2011).
939 75. S. V. Rajagopala, *et al.*, The binary protein-protein interaction landscape of
940 Escherichia coli. *Nat. Biotechnol. 2014 323* **32**, 285–290 (2014).
941 76. D. K. Orrens, C. P. Selbys, J. E. Hearst$, A. Sancars, THE JOURNAL OF
942 BIOLOGICAL CHEMISTRY Post-incision Steps of Nucleotide Excision Repair
943 in Escherichia coli DISASSEMBLY OF THE UvrBC-DNA COMPLEX BY
944 HELICASE I1 AND DNA POLYMERASE I*. *J. Biol. Chem.* **267**, 780–788

945 (1992).
946 77. P. McGlynn, R. G. Lloyd, Modulation of RNA polymerase by (p)ppGpp reveals
947 a RecG-dependent mechanism for replication fork progression. *Cell* **101**, 35–
948 45 (2000).
949 78. Y. N. Zhou, D. J. Jin, The rpoB mutants destabilizing initiation complexes at
950 stringently controlled promoters behave like “stringent” RNA polymerases in
951 Escherichia coli. *Proc. Natl. Acad. Sci. U. S. A.* **95**, 2908–2913 (1998).
952 79. E. A. Campbell, *et al.*, Structural mechanism for rifampicin inhibition of
953 bacterial rna polymerase. *Cell* **104**, 901–912 (2001).
954 80. M. Stracy, *et al.*, Live-cell superresolution microscopy reveals the organization
955 of RNA polymerase in the bacterial nucleoid. *Proc. Natl. Acad. Sci. U. S. A.*
956 **112**, E4390-9 (2015).
957 81. K. King, S. J. Benkovics, P. Modrich, THE JOURNAL OF BIOLOGICAL
958 CHEMISTRY Glu-11 1 Is Required for Activation of the DNA Cleavage Center
959 of EcoRI Endonuclease*. *J. Biol. Chem.* **264**, 11807–11815 (1989).
960 82. B. Nguyen, Y. Ordabayev, J. E. Sokoloski, E. Weiland, T. M. Lohman, Large
961 domain movements upon UvrD dimerization and helicase activation. *Proc.*
962 *Natl. Acad. Sci.* **114**, 12178–12183 (2017).
963 83. A. Wagner, Robustness against mutations in genetic networks of yeast. *Nat.*
964 *Genet. 2000 244* **24**, 355–361 (2000).
965 84. J. Atkinson, *et al.*, Localization of an accessory helicase at the replisome is
966 critical in sustaining efficient genome duplication. *Nucleic Acids Res.* **39**, 949–
967 957 (2011).
968 85. S. C. Massoni, S. J. Sandler, Specificity in suppression of SOS expression by
969 recA4162 and uvrD303. *DNA Repair (Amst).* **12**, 1072–1080 (2013).
970 86. K. H. Maslowska, K. Makiela-Dzbenska, I. J. Fijalkowska, The SOS system: A
971 complex and tightly regulated response to DNA damage. *Environ. Mol.*
972 *Mutagen.* **60**, 368–384 (2019).
973 87. R. C. Centore, S. J. Sandler, UvrD limits the number and intensities of RecA-
974 green fluorescent protein structures in Escherichia coli K-12. *J. Bacteriol.* **189**,
975 2915–2920 (2007).
976 88. V. Petrova, *et al.*, Active displacement of RecA filaments by UvrD translocase
977 activity. *Nucleic Acids Res.* **43**, 4133–4149 (2015).
978 89. M. M. Cox, Regulation of bacterial RecA protein function. *Crit. Rev. Biochem.*
979 *Mol. Biol.* **42**, 41–63 (2007).
980 90. N. Raghunathan, S. Goswami, J. K. Leela, A. Pandiyan, J. Gowrishankar, A
981 new role for Escherichia coli Dam DNA methylase in prevention of aberrant
982 chromosomal replication. *Nucleic Acids Res.* **47**, 5698–5711 (2019).
983 91. H. Yokota, Roles of the C-Terminal Amino Acids of Non-Hexameric Helicases:
984 Insights from Escherichia coli UvrD. *Int. J. Mol. Sci.* **22**, 1–19 (2021).
985 92. K. A. Datsenko, B. L. Wanner, One-step inactivation of chromosomal genes in
986 Escherichia coli K-12 using PCR products. *Proc. Natl. Acad. Sci. U. S. A.* **97**,
987 6640–6645 (2000).
988 93. J. G. Brüning, J. A. L. Howard, K. K. Myka, M. S. Dillingham, P. McGlynn, The
989 2B subdomain of Rep helicase links translocation along DNA with protein
990 displacement. *Nucleic Acids Res.* **46**, 8917–8925 (2018).
991 94. J. G. Brüning, J. A. L. Howard, P. McGlynn, Use of streptavidin bound to
992 biotinylated DNA structures as model substrates for analysis of nucleoprotein
993 complex disruption by helicases. *Methods* **108**, 48–55 (2016).
994 95. A. J. M. Wollman, A. H. Syeda, P. McGlynn, M. C. Leake, Single-Molecule

995 Observation of DNA Replication Repair Pathways in E. coli. *Adv. Exp. Med.*
996 *Biol.* **915**, 5–16 (2016).
997 96. H. Miller, *et al.*, Superresolution imaging of single DNA molecules using
998 stochastic photoblinking of minor groove and intercalating dyes. *Methods* **88**,
999 81–8 (2015).
1000 97. M. C. Leake, D. Wilson, B. Bullard, R. M. Simmons, The elasticity of single
1001 kettin molecules using a two-bead laser-tweezers assay. *FEBS Lett.* **535**, 55–
1002 60 (2003).
1003 98. M. C. Leake, D. Wilson, M. Gautel, R. M. Simmons, The elasticity of single titin
1004 molecules using a two-bead optical tweezers assay. *Biophys. J.* **87**, 1112–35
1005 (2004).
1006 99. A. J. M. Wollman, *et al.*, Critical roles for EGFR and EGFR-HER2 clusters in
1007 EGF binding of SW620 human carcinoma cells. *J. R. Soc. Interface* **19** (2022).
1008 100. M. C. Leake, *et al.*, Variable stoichiometry of the TatA component of the twin-
1009 arginine protein transport system observed by in vivo single-molecule imaging.
1010 *Proc. Natl. Acad. Sci. U. S. A.* **105**, 15376–81 (2008).
1011 101. H. Miller, *et al.*, High-Speed Single-Molecule Tracking of CXCL13 in the B-
1012 Follicle. *Front. Immunol.* **9**, 1073 (2018).
1013 102. J. Cosgrove, *et al.*, B cell zone reticular cell microenvironments shape CXCL13
1014 gradient formation. *Nat. Commun.* **11** (2020).
1015 103. X. Jin, *et al.*, Membraneless organelles formed by liquid-liquid phase
1016 separation increase bacterial fitness. *Sci. Adv.* **7** (2021).
1017 104. S.-C. Chengs, R. Kim#, K. Kings, S.-H. Kim#n, P. Modrich, THE JOURNAL OF
1018 BIOLOGICAL CHEMISTRY Isolation of Gram Quantities of EcoRI Restriction
1019 and Modification Enzymes from an Overproducing Strain*. **259**, 11571–11575
1020 (1984).
1021
1022
1023

Supplementary Information

Tetrameric UvrD helicase is located at the *E. coli* replisome due to frequent replication blocks

Adam J. M Wollman[1,2,3,], Aisha H. Syeda[1,2], Jamieson A. L. Howard[1,2], Alex Payne-Dwyer[1,2], Andrew Leech[4] , Colin Guy[5, 6], Peter McGlynn[2,6], Michelle Hawkins[2] and Mark C. Leake[1,2]

The authors wish it to be known that, in their opinion, the first two authors should be regarded as joint First Authors

[1] School of Physics, Engineering and Technology, University of York, York YO10 5DD, United Kingdom.

[2] Department of Biology, University of York, York YO10 5DD, United Kingdom.

[3] Current address: Biosciences Institute, Newcastle University, NE1 7RU, United Kingdom.

[4] Bioscience Technology Facility, Department of Biology, University of York, York YO10 5DD, United Kingdom

[5] Current address: Covance Laboratories Ltd., Otley Road, Harrogate, HG3 1PY, United Kingdom

[6] Previous address: School of Medical Sciences, Institute of Medical Sciences, University of Aberdeen, Foresterhill, Aberdeen AB25 2ZD, United Kingdom

* To whom correspondence should be addressed. To whom correspondence should be addressed. Tel: +44 (0)1904322697. Email: mark.leake@york.ac.uk

Present Address: School of Physics, Engineering and Technology, and Department of Biology, University of York, York YO10 5DD, United Kingdom

1048 **Supplementary Tables**

1049 **Table S1 Strains used in this study**

Strain	Relevant genotype	Source or derivation
BW25113 derivatives:		
BW25113	*rrnB ΔlacZ4787 hsdR514 Δ(araBAD)567 Δ(rhaBAD)568 rph-1*	(1)
JW2703	*ΔmutS::<kan>*	(1)
JW3786	*ΔuvrD::<kan>*	(1)
JW4019	*ΔuvrA::<kan>*	(1)
MG1655 derivatives:		
TB12	*ΔlacIZYA::<kan>*	
TB28	*ΔlacIZYA*	(2, 3)
TB28 derivatives		
N6577	*ΔlacIZYA Δrep::cat*	(4)
N6661	*ΔlacIZYA::<> Δrep::dhfr* / pAM407 (*uvrD*$^+$ *lacZ*$^+$, a pRC7 derivative)	(4)
N6661	*ΔlacIZYA::<> Δrep::dhfr* / pAM407 (*uvrD*$^+$ *lacZ*$^+$, a pRC7 derivative)	(4)
N6644	*ΔlacIZYA::<> uvrD::dhfr Δrep::cat* / pAM407 (*uvrD*$^+$ *lacZ*$^+$, a pRC7 derivative)	(4)
JGB166	*ΔuvrD* / pKD46	JW3786 transformed with pKD46
AS97	TB28/pKD46	(5)
AS446	*dnaQ-mCherry-<kan>*	
AS448	*dnaQ-mCherry-<>*	(5)
AS512	*mGFP-uvrD-<kan>*	*mGFP-uvrD-<kan>* recombineered into JGB166
AS517	*ΔlacIZYA::<> Δrep::cat mGFP-uvrD-<kan>* / pAM407 (*uvrD*$^+$ *lacZ*$^+$, a pRC7 derivative)	N6661 X P1(AS512)
AS564	*dnaQ-mCherry-<kan> rpoB*35*	PM486 X P1(AS446)
AS571	*dnaQ-mCherry-<> rpoB*35*	AS564 to km^S with pCP20
AS580	*dnaQ-mCherry-<> mGFP-uvrD-<kan>*	AS448 X P1(AS512)
AS582	*dnaQ-mCherry-<> mGFP-uvrD-<kan> rpoB*35*	AS571 X P1(AS512)
AS590	*dnaQ-mCherry-<> mGFP-uvrD-<kan> Δrep::cat*	AS580 X P1(N6577)
AS650	*dnaQ-mCherry-<> mGFP-uvrD-<>*	AS580 to km^S with pCP20
AS656	*dnaQ-mCherry-<> mGFP-uvrD-<> ΔuvrA::<kan>*	AS650 X P1(JW4019)
AS658	*dnaQ-mCherry-<> mGFP-uvrD-<> ΔmutS::<kan>*	AS650 X P1(JW2703)

1050

1051

1052 **Table S2 Plasmids used in this study**

Plasmid	Description	Antibiotic	Reference
pCP20	Yeast Flp recominase expression plasmid	Amp	(6)
pKD46	λ Red recombinase expression plasmid	Amp	(6)
pAS79	pUC18 *mGFP-uvrD-<kan>*	Amp, kan	This study
pAS152	pET14b-mGFP uvrD	Amp	This study

1053
1054

1055 **Table S3 Oligonucleotides used in this study**

Primer	Sequence (5' - 3')
oJGB383	TGAATGATTTTTTAGGCCAAATAAGGTGCGCAGCACCGCATCCGGCAACGCATATGAATATCCTCCTTAG
oJGB417	TACAAGACACGTGCTGAAGTC
oJGB418	TGCTAGTTGAACGCTTCCATC
oMKG71	CGGTGCCCTGAATGAACTGC
oPM319	CTTGTTGGATCAGACCGGAAAATG
oPM320	TGGCAACGCTATCCTTTTGTCA
oPM407	GCGGCAGGCAATGTGGTA
oPM409	CCTTTGAGCGTGTGGTGA
oPM411	CAGCGGCTACAAGCTCGG
oPM187B20	GTCGGATCCTCTAGACAGC(BiodT)CCATGATCACTGGCACTGGTAGAATTCGGC
oPM188B34	AACGTCATAGACGATTACATTGCTACATGGAGC(BiodT)GTCTAGAGGATCCGAC
oAS84	CCCGTCTCGATCTGGTGCAG
oAS85	TTGCTGCAAAAATCGCCCAAG
oAS132	CCCGTCTCGATCTGGTGCAGAAGAAAGGCGGAAGTTGCCTCTGGCGAGCAGGCTGGCTCCGCTGCTGG
oAS133	TTGCTGCAAAAATCGCCCAAGTCGCTATTTTTAGCGCCTTTCACAGGTATCATATGAATATCCTCCTTAG
oAS145	AGGGCGTTGCGCTTCTCCGCCCAACCTATTTTTACGCGGCGGTGCCAATGAGTAAAGGAGAAGAACTT

1056

1057

1058 **Table S4 Cell doubling times of labelled strains.** Values expressed are the means of three
1059 independent replicates, with standard deviation and standard errors indicated.

Strain (Relevant genotype)	LB medium			Minimal medium		
	Mean doubling time (min)	SD (min)	SEM (min)	Mean doubling time (min)	SD (min)	SEM (min)
WT	23.72	1.11	0.64	62.80	17.06	9.85
dnaQ-mCherry	26.85	0.91	0.52	62.22	18.63	10.76
mGFP-uvrD	24.79	0.37	0.22	59.45	1.80	1.04
dnaQ-mCherry mGFP-uvrD	25.27	1.51	0.87	71.03	7.59	4.38
ΔmutS	24.59	0.55	0.32	107.91	13.96	8.06
ΔuvrA	27.99	0.23	0.13	92.25	5.86	3.38
*ΔrpoB*35*	33.98	0.17	0.10	83.11	30.83	17.80
Δrep	24.30	2.03	1.17	62.74	1.20	0.70
dnaQ-mCherry mGFP-uvrD ΔmutS	26.85	0.68	0.39	110.84	34.91	20.16
dnaQ-mCherry mGFP-uvrD ΔuvrA	24.13	0.56	0.33	91.80	5.18	2.99
*dnaQ-mCherry mGFP-uvrD ΔrpoB*35*	32.81	0.70	0.40	99.11	78.68	45.42
dnaQ-mCherry mGFP-uvrD Δrep	26.54	1.90	1.10	62.17	2.98	1.72

1060
1061
1062
1063
1064

1065

1066 **Supplementary figures**

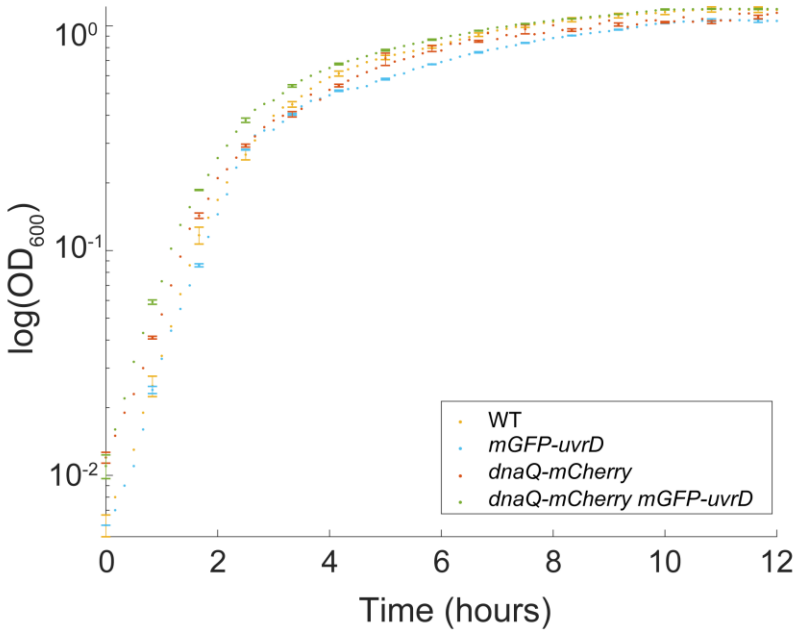

1067

1068

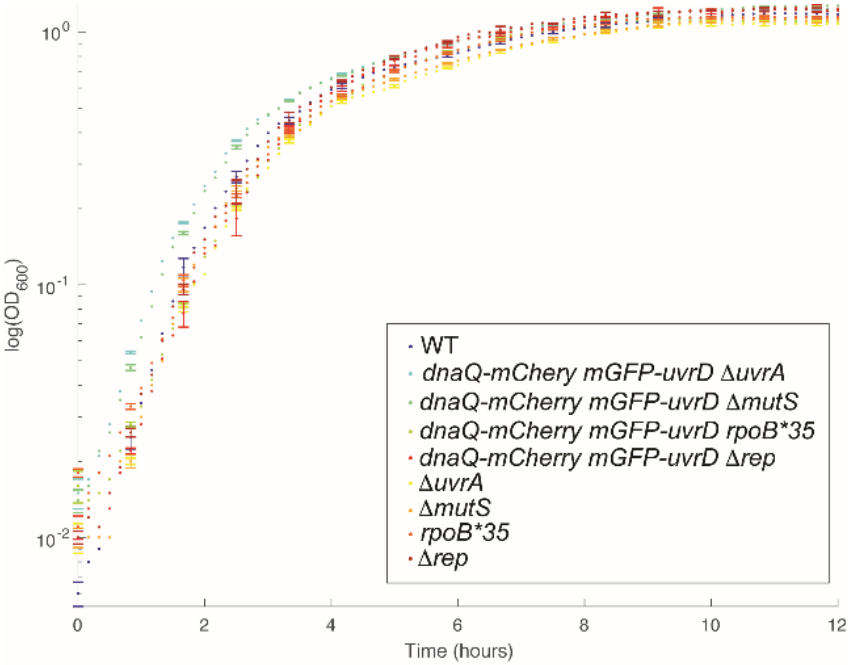

1069

1070 **Supplementary Figure S1. Growth curves in LB medium.** Cultures were grown in LB as
1071 described in the text. The OD_{600} values are plotted on a log scale on the vertical axis with a
1072 linear scale of time in hours on the horizontal axis. The genotypes of the strains are indicated
1073 in boxes within the figures. SD error bars (shown just on every 5th consecutive point for clarity
1074 here), taken from N=3 replicate cultures. Plots in panel A are growth curves of single and dual
1075 labelled wild-type strains, while those in panel B are dual labelled and unlabelled mutant
1076 strains. The unlabelled wild-type strain is included in all panels as a reference.

1077

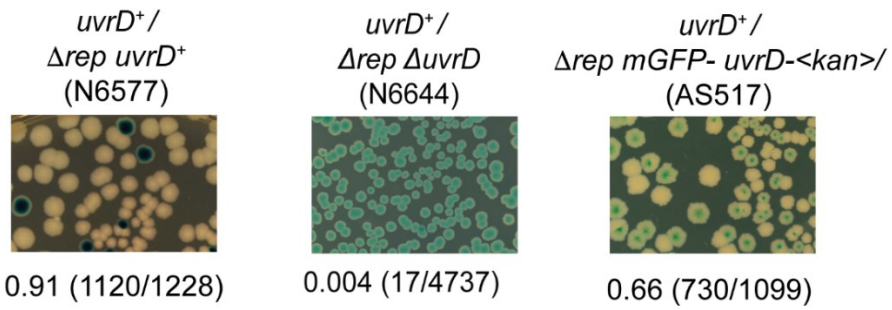

1078

1079 **Supplementary Figure S2: Testing of mGFP-UvrD fusions for retention of function.** We
1080 transformed the strain carrying a chromosomal *mGFP-uvrD* allele with a derivative of pRC7
1081 carrying a wild-type *uvrD* allele (pPM407), which is an unstable low copy plasmid that also
1082 carries the *lacZYA* genes (3). Presence of this plasmid confers blue colour to the colonies on
1083 plates containing Xgal when strains are chromosomally deleted for the *lac* operon. In rapidly
1084 growing cells, cells require either *rep* or *uvrD* for viability, and the loss of both is lethal (4, 7).
1085 Thus, *Δrep* cells with a functional *uvrD* allele are viable and can lose pRC7*uvrD*, evidenced
1086 by appearance of white colonies on LB Xgal IPTG plates, but cells lacking *uvrD* function
1087 cannot survive upon loss of the plasmid resulting in recovery of only blue colonies. The *Δrep*
1088 *mGFP-uvrD* cells produced white colonies on Xgal media, indicating that the *mGFP-uvrD*
1089 fusion is functional.
1090

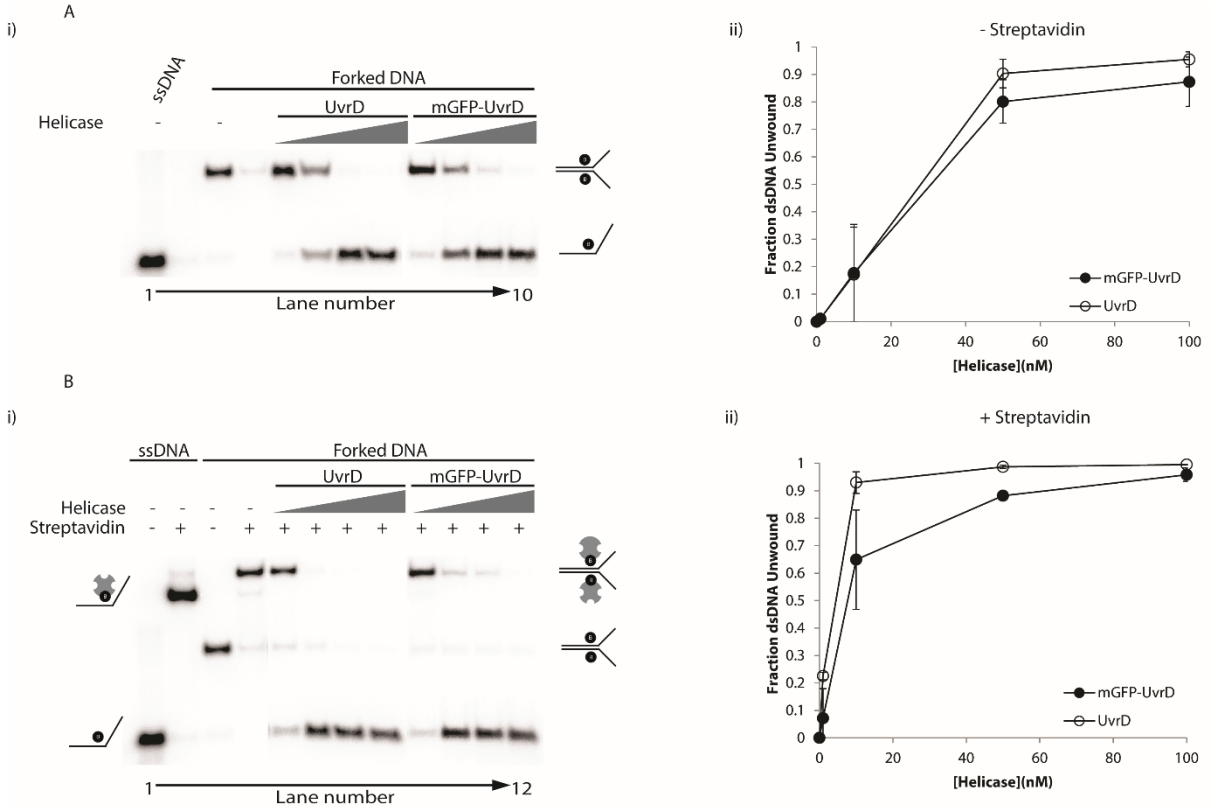

Supplementary Figure S3: mGFP-UvrD fusion is functional *in vitro*. (A)(i) Representative native polyacrylamide TBE gel showing UvrD and mGFP-UvrD unwinding of forked DNA containing biotin on both strands within the duplex region (8, 9). Lanes 1-2 contain markers indicating the position of single stranded or forked DNA as indicated. Lanes 3-10 contain the products of unwinding the forked DNA by the indicated helicase at 1, 10, 50 and 100 nM. (ii) Quantification of the unwinding of the forked substrate by the indicated helicases. Data points shown are averages of band intensities (taken from two gels in UvrD and four gels in mGFP-UvrD) with standard errors indicated by bars on the points. (B)(i) Representative native polyacrylamide TBE gels showing UvrD and mGFP-UvrD unwinding of forked DNA containing biotin on both strands within the duplex region (8, 9). Lanes 1-4 contain markers indicating the position of single stranded or forked DNA +/- streptavidin as indicated. Lanes 5-12 contain the products of unwinding the forked DNA +/- streptavidin by the indicated helicase at 1, 10, 50 and 100 nM. (ii) Quantification of the unwinding of the forked substrate in the presence of streptavidin by the indicated helicases. Data points shown are averages of band intensities (taken from two gels in UvrD and four gels in mGFP-UvrD) with standard errors indicated by bars on the points.

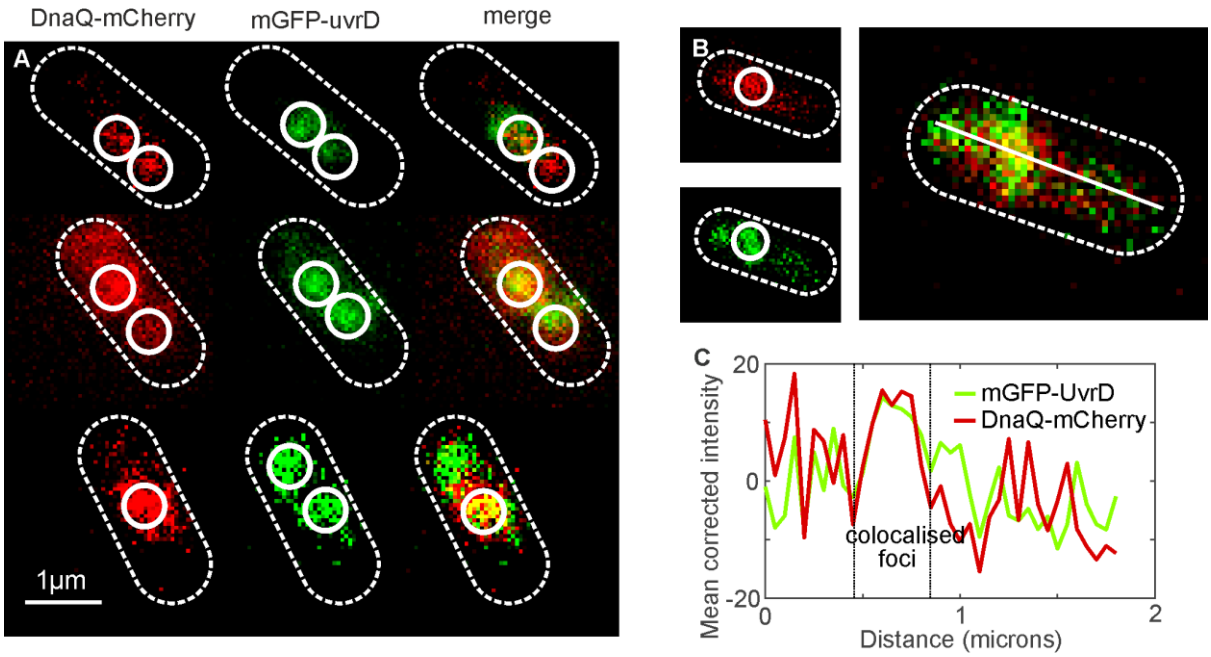

Supplementary Figure S4: A. and B. Dual colour Slimfield images of mGFP-UvrD:DnaQ-mCherry, scale bar 1 micron. Segmented outlines of cell bodies (white dash) and detected foci (white circles) indicated. C. Mean corrected intensity line profile through a colocalized foci in B.

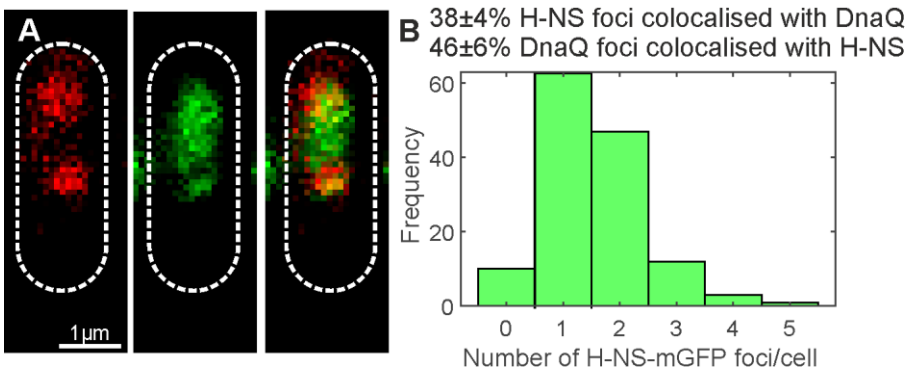

Supplementary Figure S5: (A) Dual colour Slimfield images of H-NS-mGFP-:DnaQ-mCherry, scale bar 1 micron. Segmented outlines of cell bodies indicated (white dash). (B) Histogram showing the number of H-NS foci detected per cell, SD errors.

1120

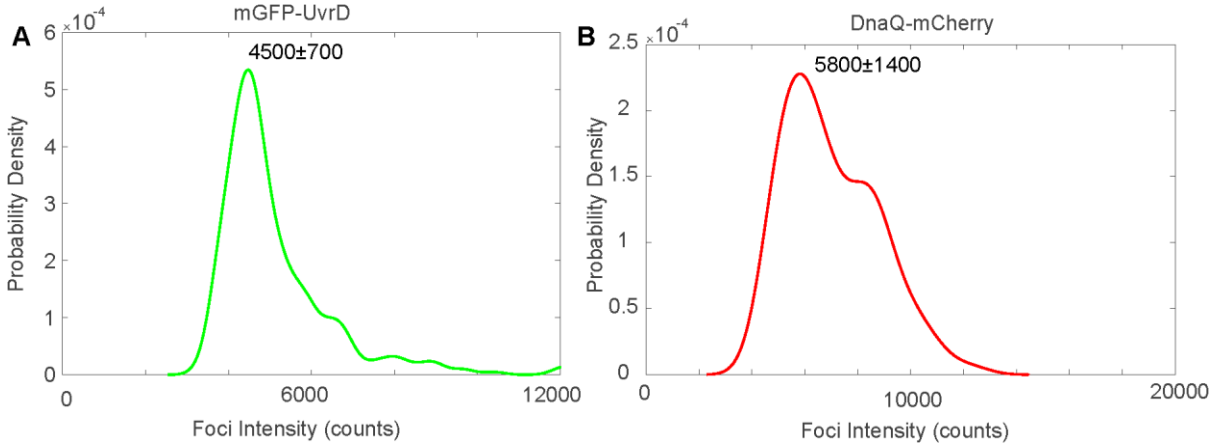

1121

1122 **Supplementary Figure S6: Brightness of single mGFP and mCherry molecules** A. and
1123 B. Characteristic intensity distributions rendered as kernel density estimates of single mGFP-
1124 UvrD and DnaQ-mCherry obtained using Slimfield imaging. Peak±full width at half maximum
1125 indicated. Distributions calculated from the tracked foci intensity distributions from the end of
1126 the photobleach process such that only single fluorophore molecules are detected. Number
1127 of molecules per foci before bleaching is determined by dividing the initial foci intensity by
1128 these values for the equivalent fluorophore.

1129

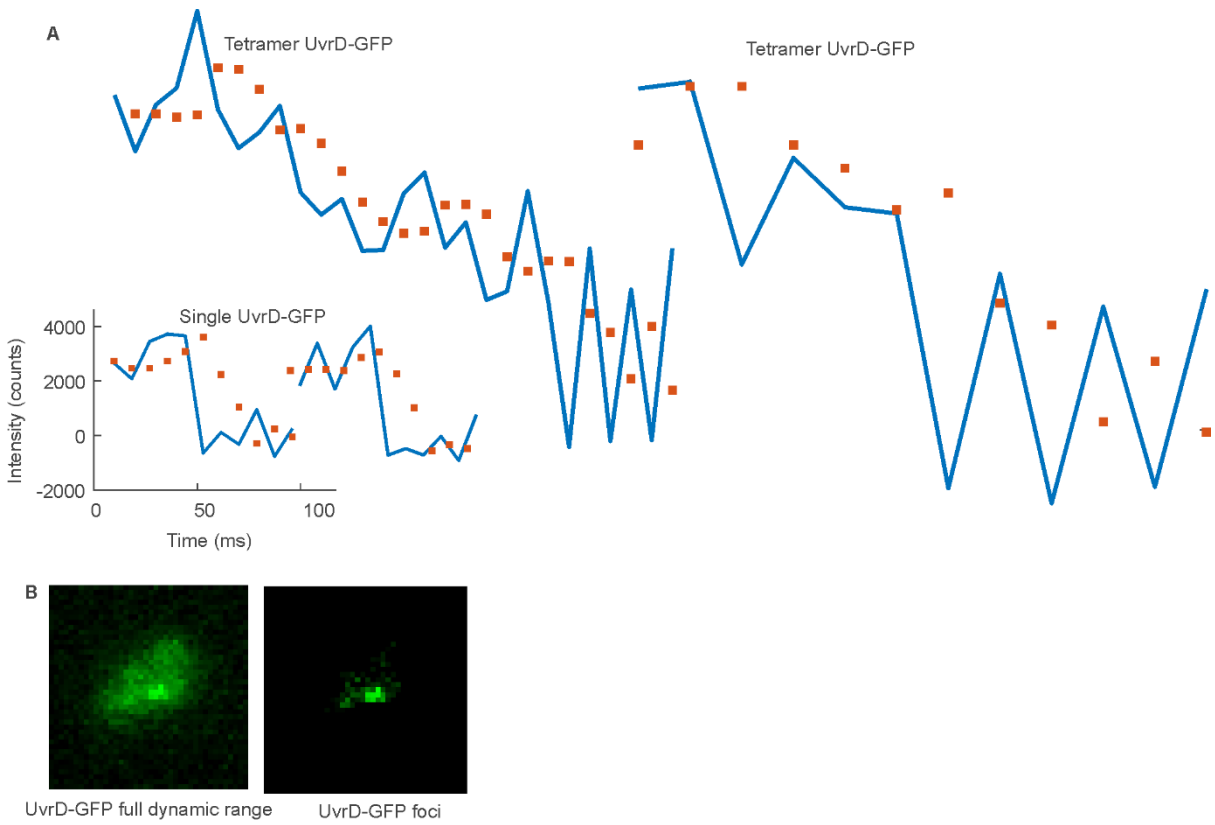

Supplementary Figure S7: Single-molecule image analysis. A. Chung-Kennedy filtered (squares) intensity traces for single UvrD tracks showing tetramers exhibiting multiple photobleach steps and monomers detected towards the end of photobleaching. Foci were 'overtracked' beyond the last detected bright frame to illustrate steps. **B**. UvrD-GFP micrograph showing the full dynamic range (left) and adjusted to illustrate a foci (right)

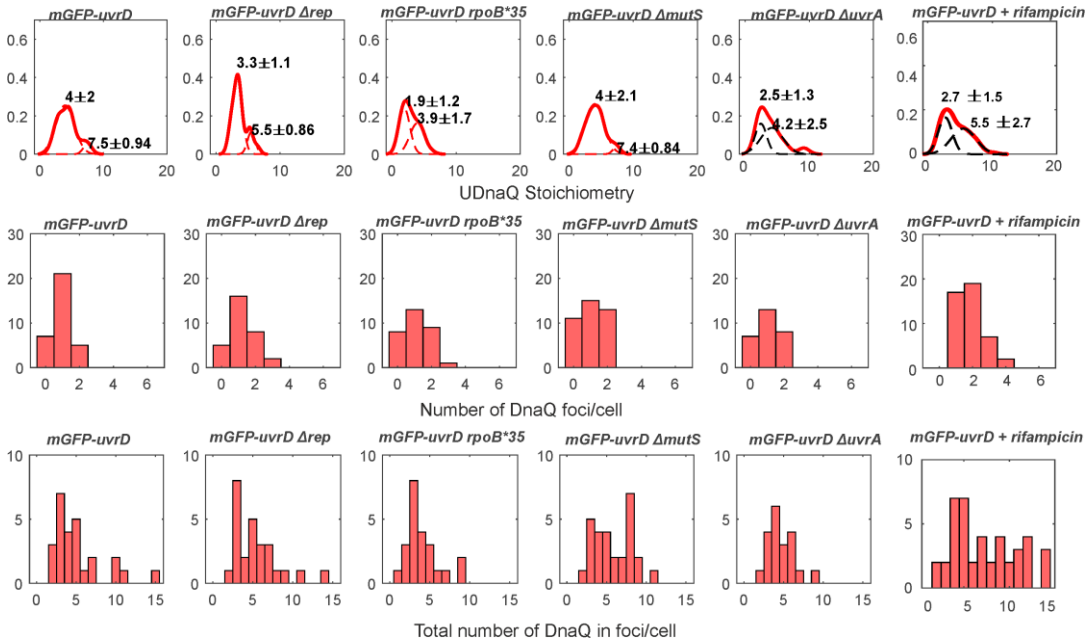

Supplementary Figure S8: DnaQ tracking characterization. Top row: Distribution of DnaQ foci stoichiometry as a kernel density estimate for all strains and conditions (red) with two Gaussian fit overlaid as black dotted lines. Peak ± half width at half maximum shown above. Middle row: Corresponding histogram of number of foci detected per cell. Bottom row: histogram of the total amount of DnaQ in foci per cell. N=30-50 cells per strain or condition.

1150

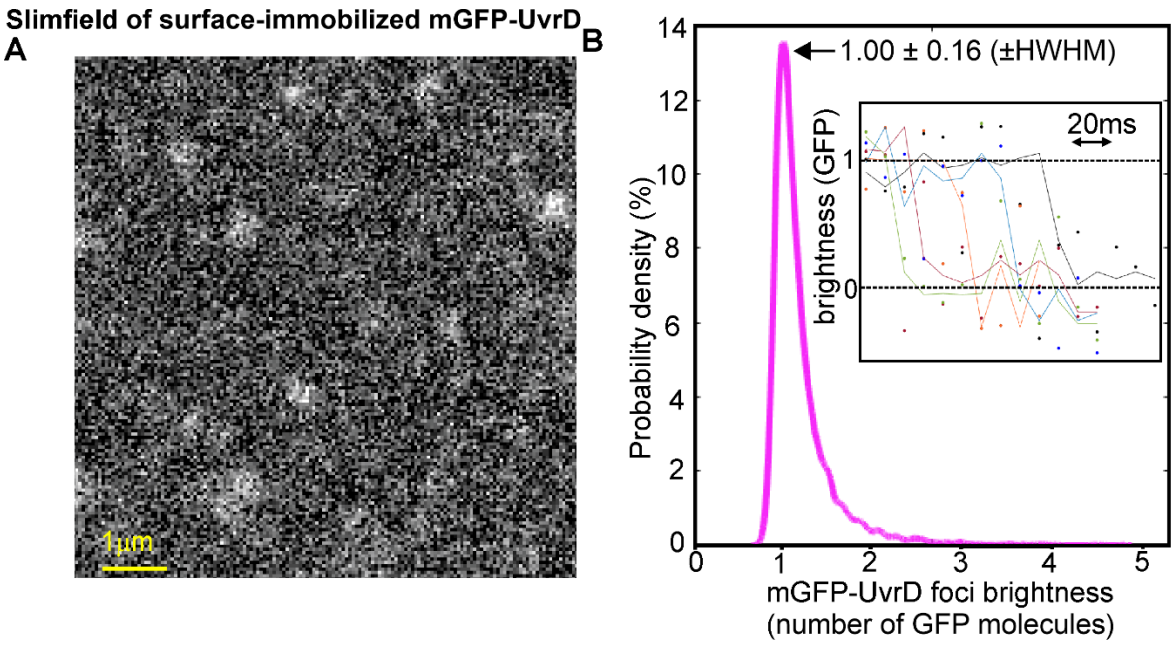

1151
1152
1153 **Supplementary Figure S9: Single-molecule microscopy of purified mGFP-UvrD.** A.
1154 Representative Slimfield image of surface-immobilized mGFP-UvrD. B. Automated single-
1155 particle tracking output for mGFP-UvrD showing probability distribution for mGFP-UvrD foci
1156 brightness normalized by the single-molecule dye brightness, peak (±HWHM) corresponding
1157 to 1 molecule indicated (arrow) for n=7,384 foci. *Inset*: example overlaid stepwise
1158 photobleach traces for four different mGFP-UvrD foci indicating a consistent single-molecule
1159 step to zero brightness whose size is comparable to the measured modal brightness across
1160 all foci (dots: raw data, lines: Chung-Kennedy edge-preserving filter output).
1161
1162

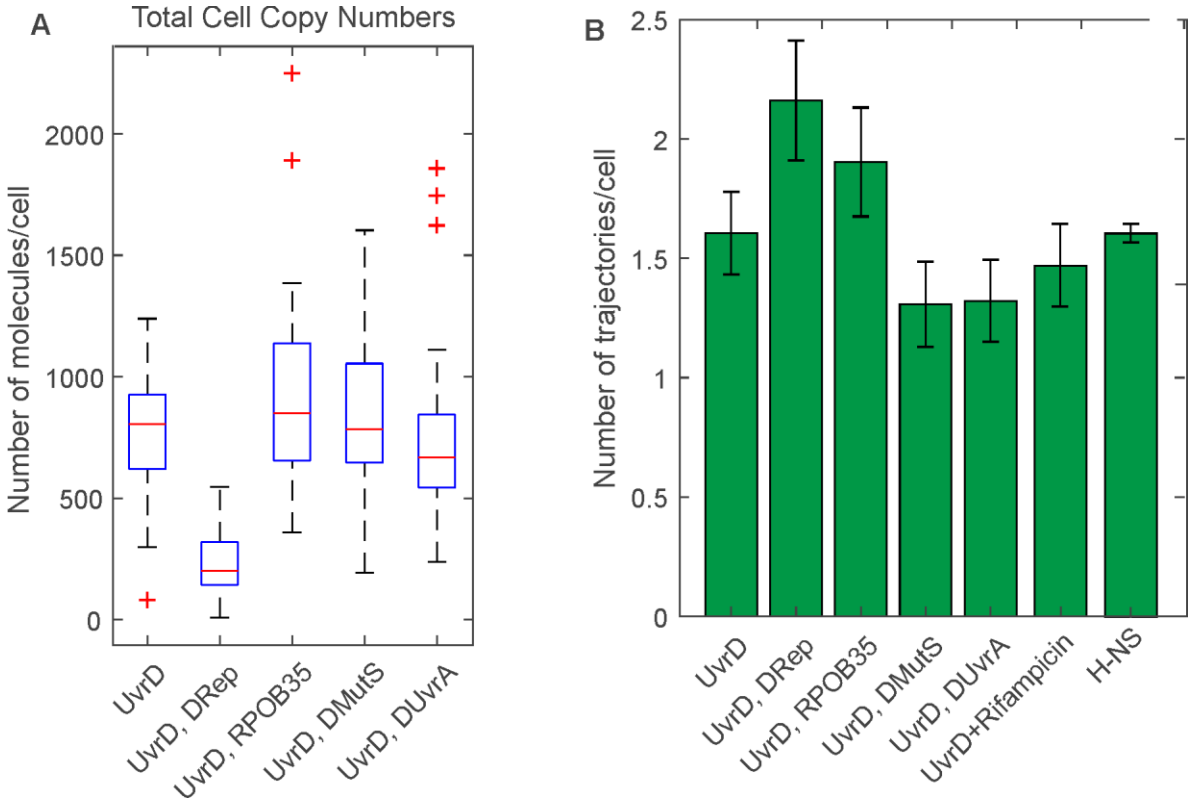

Supplementary Figure S10: A. Boxplot of the total number of mGFP-UvrD molecules per cell, estimated by numerical integration of the whole cell fluorescence. Median is shown as red line, bottom and top of the blue box mark the 25th and 75th percentiles and whiskers extend to the most extreme points not considered outliers (2.7 standard deviations covering 99.3% of normally distributed data) with outliers beyond this shown as red +. N=30 cells per strain. B Number of trajectories per cell used in the stoichiometry determination

1173

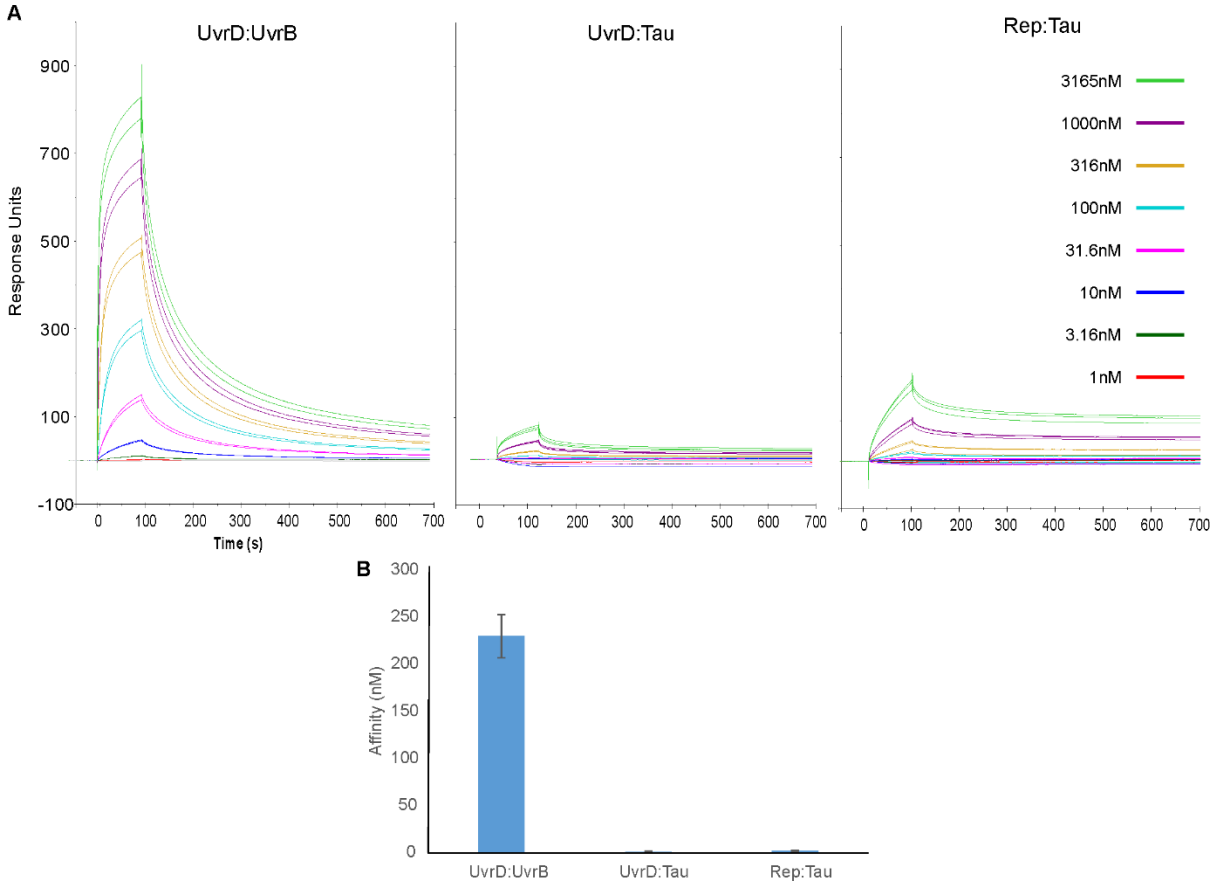

1174

1175 **Supplementary Figure S11: Surface plasmon resonance measurements of helicase**
1176 **interactions with Tau** A. Titration response curves for UvrD:UvrB, UvrD:Tau and Rep:Tau
1177 with their affinities shown in B.

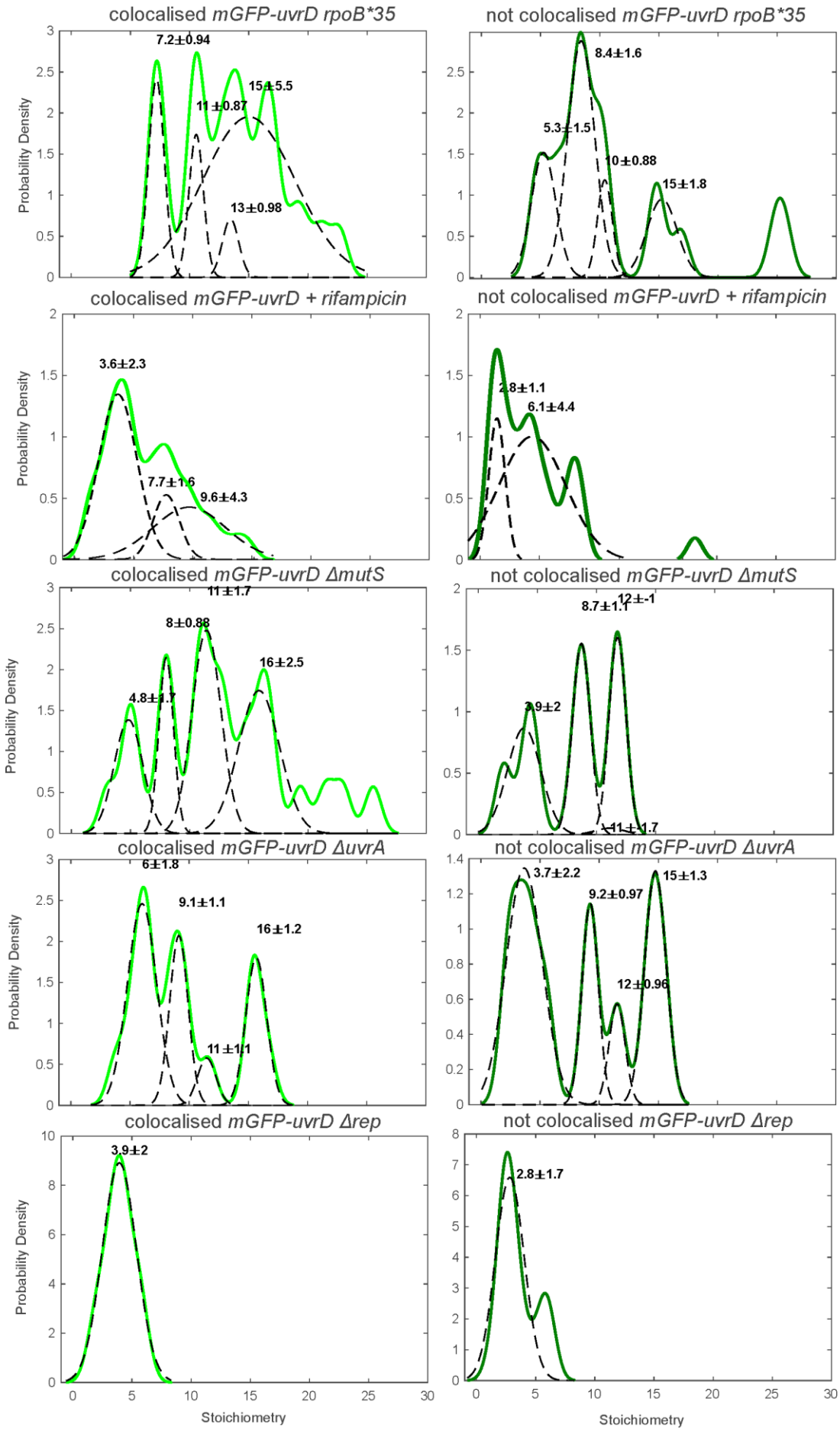
colocalised mGFP-uvrD rpoB*35
7.2±0.94
11±0.87
15±5.5
13±0.98
not colocalised mGFP-uvrD rpoB*35
8.4±1.6
5.3±1.5
10±0.88
15±1.8
colocalised mGFP-uvrD + rifampicin
3.6±2.3
7.7±1.6
9.6±4.3
not colocalised mGFP-uvrD + rifampicin
2.8±1.1
6.1±4.4
colocalised mGFP-uvrD ΔmutS
11±1.7
8±0.88
16±2.5
4.8±1.7
not colocalised mGFP-uvrD ΔmutS
8.7±1.1
12±-1
3.9±2
11±1.7
colocalised mGFP-uvrD ΔuvrA
6±1.8
9.1±1.1
16±1.2
11±1.1
not colocalised mGFP-uvrD ΔuvrA
3.7±2.2
9.2±0.97
15±1.3
12±0.96
colocalised mGFP-uvrD Δrep
3.9±2
not colocalised mGFP-uvrD Δrep
2.8±1.7
Probability Density
Stoichiometry

1178

1179 **Supplementary Figure S12:** Perturbed UvrD stoichiometry. The distribution of UvrD foci
1180 stoichiometry rendered as a kernel density estimate for foci colocalised (Left) and non-
1181 colocalised (Right) with DnaQ foci. Distributions were fitted with multiple Gaussian fits (black
1182 dotted lines) with the peak value ± half width at half maximum indicated above each peak.
1183

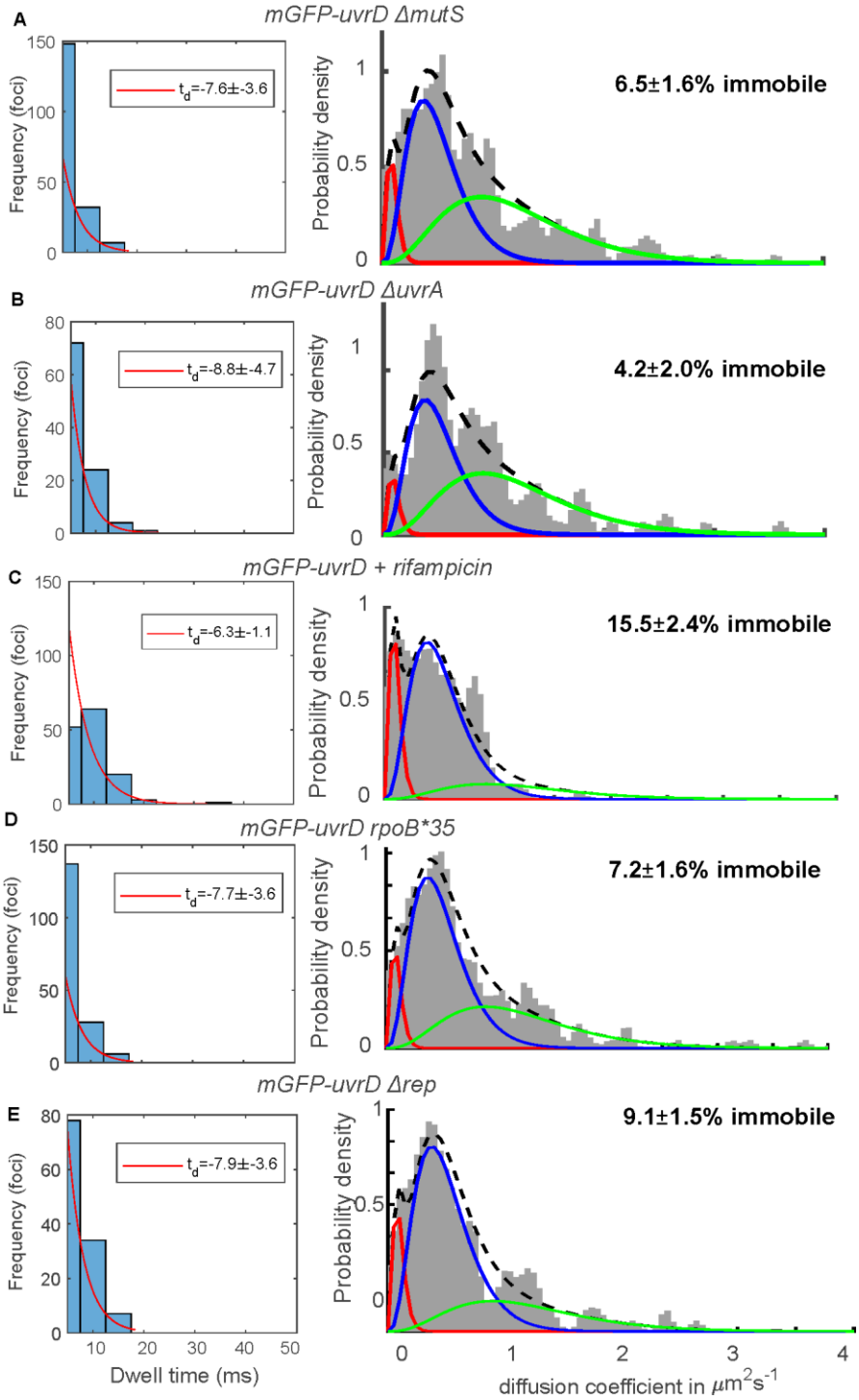

Supplementary Figure S13: UvrD perturbed dynamics. A-E Left, distribution of time UvrD and DnaQ foci were colocalised (blue) fit with an exponential (red) to yield a characteristic dwell time. Right, distribution of microscopic diffusion coefficients of UvrD foci (grey) fitted with a three state gamma distribution model containing a relatively immobile population with D = 0.1 μm^2/s (red), a transiently immobile population, D = 0.5 μm^2/s (blue) and a mobile population, D=1.2 μm^2/s (green). Errors represent 95% confidence intervals. N~300 foci/condition.

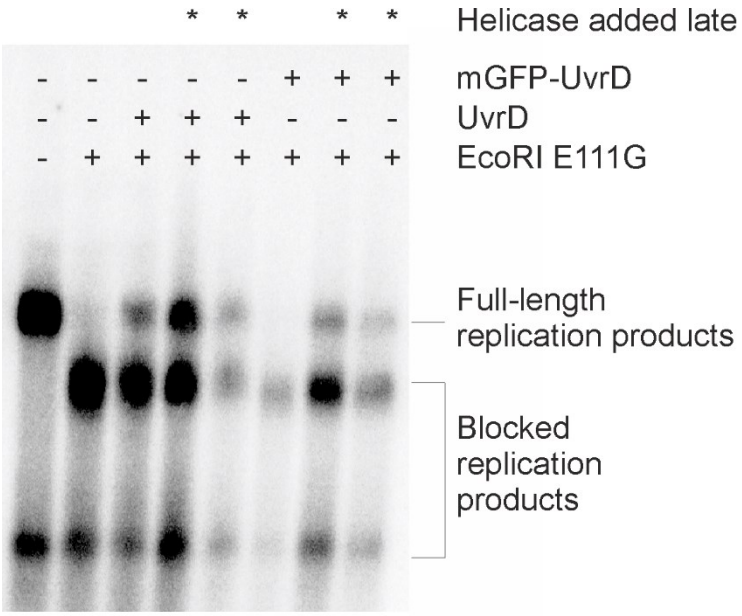

Supplementary Figure S14: In vitro replication assay using mGFP-UvrD. Denaturing agarose gel of replication products formed from pPM872 (1) in the absence and presence of EcoRI E111G block, mGFP-UvrD and UvrD added pre- and post-collision (*) as indicated.

1199 **Supplementary references**
1200

1201 1. Baba,T., Ara,T., Hasegawa,M., Takai,Y., Okumura,Y., Baba,M., Datsenko,K.A.,
1202 Tomita,M., Wanner,B.L. and Mori,H. (2006) Construction of Escherichia coli K-12 in-
1203 frame, single-gene knockout mutants: the Keio collection. *Mol. Syst. Biol.*, **2**,
1204 2006.0008.
1205 2. Bachmann,B.J. (1996) Derivations and genotypes of some mutant derivatives
1206 of Escherichia coli K-12. . In Neidhardt,F.C., Curtiss III,R., Ingraham,J.L., Lin,E.C.C.,
1207 Low,K.B., Magasanik,B., Reznikoff,W.S., Riley,M., Schaechter,M., Umbarger,H.E.
1208 (eds), *Escherichia coli and Salmonella cellular and molecular biology*. ASM Press,
1209 Washington, DC, pp. 2460–2488.
1210 3. Bernhardt,T.G. and de Boer,P.A.J. (2004) Screening for synthetic lethal mutants in
1211 Escherichia coli and identification of EnvC (YibP) as a periplasmic septal ring factor
1212 with murein hydrolase activity. *Mol. Microbiol.*, **52**, 1255–1269.
1213 4. Guy,C.P., Atkinson,J., Gupta,M.K., Mahdi,A.A., Gwynn,E.J., Rudolph,C.J., Moon,P.B.,
1214 van Knippenberg,I.C., Cadman,C.J., Dillingham,M.S., *et al.* (2009) Rep provides a
1215 second motor at the replisome to promote duplication of protein-bound DNA. *Mol.*
1216 *Cell*, **36**, 654–666.
1217 5. Syeda,A.H., Wollman,A.J.M., Hargreaves,A.L., Howard,J.A.L., Brüning,J.-G., McGlynn,P.
1218 and Leake,M.C. (2019) Single-molecule live cell imaging of Rep reveals the dynamic
1219 interplay between an accessory replicative helicase and the replisome. *Nucleic Acids*
1220 *Res.*, **47**, 6287–6298.
1221 6. Datsenko,K.A. and Wanner,B.L. (2000) One-step inactivation of chromosomal genes in
1222 *Escherichia coli* K-12 using PCR products. *Proc. Natl. Acad. Sci. USA*, **97**, 6640–
1223 6645.
1224 7. Boubakri,H., de Septenville,A.L., Viguera,E. and Michel,B. (2010) The helicases DinG,
1225 Rep and UvrD cooperate to promote replication across transcription units in vivo.
1226 *EMBO J.*, **29**, 145–157.
1227 8. Brüning,J.-G., Howard,J.A.L. and McGlynn,P. (2016) Use of streptavidin bound to
1228 biotinylated DNA structures as model substrates for analysis of nucleoprotein
1229 complex disruption by helicases. *Methods*, **108**, 48–55.
1230 9. Brüning,J.-G., Howard,J.A.L., Myka,K.K., Dillingham,M.S. and McGlynn,P. (2018) The 2B
1231 subdomain of Rep helicase links translocation along DNA with protein displacement.
1232 *Nucleic Acids Res.*, **46**, 8917–8925.

1233
1234